



저작자표시-비영리-변경금지 2.0 대한민국

이용자는 아래의 조건을 따르는 경우에 한하여 자유롭게

- 이 저작물을 복제, 배포, 전송, 전시, 공연 및 방송할 수 있습니다.

다음과 같은 조건을 따라야 합니다:



저작자표시. 귀하는 원저작자를 표시하여야 합니다.



비영리. 귀하는 이 저작물을 영리 목적으로 이용할 수 없습니다.



변경금지. 귀하는 이 저작물을 개작, 변형 또는 가공할 수 없습니다.

- 귀하는, 이 저작물의 재이용이나 배포의 경우, 이 저작물에 적용된 이용허락조건을 명확하게 나타내어야 합니다.
- 저작권자로부터 별도의 허가를 받으면 이러한 조건들은 적용되지 않습니다.

저작권법에 따른 이용자의 권리는 위의 내용에 의하여 영향을 받지 않습니다.

이것은 [이용허락규약\(Legal Code\)](#)을 이해하기 쉽게 요약한 것입니다.

[Disclaimer](#)

Ph.D. Dissertation of Medical Science

**rt269L-Type Hepatitis B virus (HBV)
in genotype C infection leads to
improved mitochondrial dynamics via
the PERK-eIF2 α -ATF4 axis in an HBx
protein-dependent manner**

HBV 유전자형 C rt269L 타입 감염의
HBx 단백 의존적 PERK-eIF2 α -ATF4
신호 유도를 통한 개선된 미토콘드리아 역학 규명

August 2023

**The Department of Biomedical sciences
Seoul National University
College of Medicine**

Yumin Choi

**rt269L-Type Hepatitis B virus (HBV)
in genotype C infection leads to
improved mitochondrial dynamics via
the PERK-eIF2 α -ATF4 axis in an HBx
protein-dependent manner**

Advisor: Prof. Bum-Joon Kim

**Submitting a Ph.D. Dissertation of
Medicine**

August 2023

**The Department of Biomedical sciences
Seoul National University
College of Medicine**

Yumin Choi

**Confirming the Ph.D. Dissertation written by
Yumin Choi**

HBV 유전자형 C rt269L 타입 감염의
HBx 단백질 의존적 PERK-eIF2 α -ATF4
신호 유도를 통한 개선된 미토콘드리아 역학 규명

지도교수 김 범 준

이 논문을 의학박사 학위논문으로 제출함

2023년 6월

서울대학교 대학원
의과학과 의과학 전공
최 유 민

최유민의 박사 학위논문을 인준함

2023년 6월

위 원 장 _____ 조남혁 _____ (인)
부위원장 _____ 김범준 _____ (인)
위 원 _____ 석승혁 _____ (인)
위 원 _____ 유수중 _____ (인)
위 원 _____ 장원중 _____ (인)

**rt269L-Type Hepatitis B virus (HBV)
in genotype C infection leads to
improved mitochondrial dynamics via
the PERK-eIF2 α -ATF4 axis in an HBx
protein-dependent manner**

Yumin Choi

Advisor: Prof. Bum-Joon Kim

**A thesis submitted to the Department of Biomedical Sciences
in partial fulfillment of the requirements for the
Degree of Doctor of Philosophy in Medical Science at
Seoul National University College of Medicine**

June 2023

Approved by Thesis Committee:

Chairman Nam-Hyuk Cho (Seal)

Vice Chairman Bum-Joon Kim (Seal)

Professor Seung Hyeok Seok (Seal)

Professor Su Jong Yu (Seal)

Professor Won-Jong Jang (Seal)

Abstract

rt269L-Type Hepatitis B virus (HBV) in genotype C infection leads to improved mitochondrial dynamics via the PERK-eIF2 α -ATF4 axis in an HBx protein-dependent manner

Yumin Choi

Department of Biomedical Sciences

Seoul National University College of Medicine

Background: In the previous report, the rt269I type versus the rt269L type in genotype C2 infection led to poor clinical outcomes and enhanced mitochondrial stress in infected hepatocytes. Here, I sought to investigate differences between the rt269L and rt269I types in mitochondrial functionality in HBV genotype C2 infection, mainly focusing on ER stress-mediated autophagy induction as an upstream signal.

Methods: Mitochondrial functionality, ER stress signaling, autophagy induction, and apoptotic cell death between rt269L type and rt269I type groups were investigated via *in vitro* and *in vivo* experiments. Serum

samples were collected from 187 chronic hepatitis patients who visited Konkuk or Seoul National University Hospital.

Results: The data revealed that genotype C rt269L versus rt269I infection led to improved mitochondrial dynamics and enhanced autophagic flux, mainly due to the activation of the PERK–eIF2 α –ATF4 axis. Furthermore, I demonstrated that the traits found in genotype C rt269L infection were mainly due to increased stability of the HBx protein after deubiquitination. In addition, clinical data using patient sera from two independent Korean cohorts showed that compared to rt269I, rt269L in infection led to lower 8-OHdG levels, further supporting its improved mitochondrial quality control.

Conclusion: The data showed that compared to the rt269I type, the rt269L type, which presented exclusively in HBV genotype C infection, leads to improved mitochondrial dynamics or bioenergetics, mainly due to autophagy induction via activation of the PERK–eIF2 α –ATF4 axis in an HBx protein-dependent manner. This suggests that HBx stability and cellular quality control in the rt269L type predominating in genotype C endemic areas could at least partly contribute to some distinctive traits of genotype C infection, such as higher infectivity or longer duration of the HBeAg positive stage.

* This study included data previously published in Cellular & Molecular Biology Letters (2023)

Keyword: Mitochondrial functionality; ER stress; Autophagy; HBx stability; Deubiquitination

Student Number: 2017-24402

Table of Contents

Abstract	i
Contents.....	iv
List of figures	v
List of tables	viii
List of abbreviations	ix
Introduction	1
Materials and Methods	5
Results.....	21
Discussions.....	72
Conclusions	77
References.....	79
Abstract in Korean	83

List of Figures

Figure 1. rt269L-infected cells showed improved mitochondrial maintenance with a high rate of functional mitochondria and biogenesis	23
Figure 2. Confocal microscopy images showing HepG2 cells transfected with mock, rt269L, or rt269I HBV followed TMRM staining indicating mitochondrial outer membrane permeabilization (MOMP) and $\Delta\Psi_m$	24
Figure 3. rt269L-infected cells showed improved mitochondrial bioenergetics with a high rate of functional mitochondria and biogenesis.....	25
Figure 4. rt269L induced increased mtDNA gene transcription as well as increased PGC-1α protein expression.....	27
Figure 5. rt269L activates the PERK-mediated UPR pathway, but an impaired UPR is shown in rt269I-infected cells.....	30
Figure 6. Immunohistochemical analysis of p-eIF2α expression (red arrow) in paraffin-embedded liver tissues	31
Figure 7. rt269L activates PERK-peIF2α-ATF4 signaling.....	32
Figure 8. rt269L genotype C HBV infection led to enhanced autophagy induction.....	35
Figure 9. rt269L genotype C HBV infection led to enhanced autophagy induction.....	37
Figure 10. EGFP-LC3 assay with flow cytometry.....	38
Figure 11. Enhanced autophagy in rt269L HBV infection.....	39
Figure 12. Comparison of autophagy/mitophagy induction in genotype A and C HBV infection.....	40
Figure 13. HBx in rt269L strongly interact with PI3KC3 (VPS34).....	42

Figure 14. Immunofluorescence for the colocalization of autophagosomes with mitochondria.....	43
Figure 15. rt269I induces caspase activation and cell death by releasing cytochrome c.....	47
Figure 16. rt269I HBV induces caspase activation and cell death.....	48
Figure 17. Detection of intracellular reactive oxygen species in hepatocytes transfected with rt269L or rt269I HBV.....	49
Figure 18. rt269I induces caspase activation and cell death.....	50
Figure 19. Cell death in liver tissues of mice hydrodynamically injected with the mock, rt269L, or rt269I vector was detected by TUNEL assay.....	51
Figure 20. rt269L leads to increased HBx protein stability.....	53
Figure 21. rt269L leads to increased HBx protein stability in both genotype A and C.....	54
Figure 22. rt269L type HBV infection in both genotype C and A activated phospho-Akt and phospho-PI3K signals.....	56
Figure 23. rt269L type HBV infection activated phospho-mTOR and phospho-PI3K signals in HBx protein dependent manner.....	57
Figure 24. rt269L attenuates HBx degradation through ubiquitination of HBx.....	61
Figure 25. Site-directed mutagenesis to introduce a stop codon downstream of the Polymerase start region.....	63
Figure 26. HBV Pol genome and the proteins it encodes are critical for HBx production and ubiquitination.....	64
Figure 27. Site-directed mutagenesis to introduce a stop codon upstream of the rt269 region.....	65

Figure 28. Elevated hepatic oxidative damage in rt269I HBV infection and its clinical implications.....68

Schematic Figure78

List of Tables

Table 1. PCR primers used in this study	18
Table 2. List of Antibodies.....	19
Table 3. Comparison of clinical factors between two variants in the rt269 codon (KU cohort)	70
Table 4. Comparison of clinical factors between two variants in the rt269 codon (SNU cohort)	71

List of Abbreviations

mtDNA: Mitochondrial DNA

HBeAg: Hepatitis B e antigen

HCC: Hepatocellular carcinoma

ROS: reactive oxygen species

8-OHdG: 8-Hydroxy-2'-deoxyguanosine

PERK: Protein kinase R (PKR)-like ER kinase

ATF6: Activating transcription factor 6

IRE1 α : Inositol-requiring enzyme 1 alpha

ATF4: Activating Transcription Factor 4

XBP1: X-Box Binding Protein 1

LC3: Microtubule-associated protein 1 light chain 3 beta

UPR: Unfolded protein response

ER: endoplasmic reticulum

HBx: Hepatitis B X protein

RT: Reverse Transcriptase

TMRM: tetramethylrhodamine methyl ester

nDNA: Nuclear DNA

EGFP: Enhanced Green Fluorescent Protein

Introduction

Hepatitis B virus (HBV) infection is a major cause of chronic liver disease, including liver cirrhosis (LC), hepatic decompensation, and hepatocellular carcinoma (HCC) [1, 2]. Despite effective HBV vaccines and life cycle inhibitors, the annual number of HBV-related liver disease deaths is approximately 820,000 worldwide [3]. Based on the genetic divergence of the HBV genomic sequences, 10 HBV genotypes (from A to J) and derived subtypes have been identified. The major genotypes diverge in terms of geographical distribution. Genotype A is most common in America, Africa, Europe and India. Genotype B and C are highly prevalent in the Asia–Pacific region. Genotype D is widespread in Africa, Europe, India, and the Mediterranean region. Genotype E is limited to West and Central Africa and Saudi Arabia. Genotype F is present in Central and South America, Mexico. Genotype G has been found in the Americas, France, and Germany. Genotype H has been identified in Central America, Mexico. Genotype I is restricted to Laos and Vietnam. Genotype J is found in Japan [4, 5]. Among the 10 (A-J) HBV genotypes, infection with genotype C carries a greater risk for severe liver disease progression, with clinical features of prolonged active disease and delayed hepatitis B e antigen (HBeAg) seroconversion [6,

7]. Although clinical data and knowledge indicate poor prognosis for people with HBV genotype C infection, much remains unknown and requires clarification.

A substantial level of research has reported that there are clinical relationships between HBV infection and mitochondrial function. Since HBV does not have a metabolic system, it is crucial for HBV to utilize and control cell signal transduction for replication cycle success. Mitochondria are the most important intracellular organelles in cellular energy production and engage in key intracellular interactions with other organelles.

Mitochondria can adapt to hostile cell environments by mitochondrial dynamics and mitophagy to maintain their homeostasis [8, 9]. Disruption of normal mitochondrial dynamics mainly induced by pathological conditions, such as cancers and viral infection, can cause mitochondrial damage, leading to loss of its membrane potential and release of mitochondrial contents, including mitochondrial DNA (mtDNA) and/or ROS, into blood, which ultimately cause proapoptotic or necrotic events [10, 11].

Mitochondrial damage and oxidative stress are prominent features of HBV infection. Furthermore, some preS or HBsAg variants causing ER stress-mediated liver disease progression have been reported to lead to mitochondrial dysfunction [12]

Recently, protein kinase R (PKR)-like ER kinase (PERK), an endoplasmic reticulum (ER) stress sensor involved in the unfolded protein response (UPR), has been reported to protect mitochondrial homeostasis during ER stress [13-15]. Activation of PERK-eIF2 α -ATF4 can strengthen mitochondrial quality control by increasing mitochondrial biogenesis and mitophagy, resulting in renewal of the mitochondrial network [16].

There are two polymorphisms in HBV polymerase, rt269L and rt269I, in genotype C infection, distinct from other genotypes, of which most infection is due to a single rt269I type. Previously, I reported that the rt269I type leads to enhanced mitochondrial stress and was associated with a significantly greater extent with HBeAg-negative seroconversion and liver disease progression in genotype C infections than the rt269L type [17]. I also recently revealed that rt269I is more prone to mutation in the genotype C2 genome than rt269L, suggesting that the former could induce enhanced immune pressure during chronic infections [18]. Together, these results suggest that there may be definitely different capacities to maintain mitochondrial homeostasis between rt269L and rt269I types in genotype C infection. Elucidation of its underlying mechanism at the molecular level could provide a deeper understanding regarding distinct clinical and virological traits of HBV C infection. So. In the present study, I sought to

investigate differences between the rt269L and rt269I types in mitochondrial functionality in HBV genotype C2 infection, mainly focusing on ER stress-mediated autophagy induction as its upstream signal.

Materials and Methods

Cells and Reagents

Human hepatocellular carcinoma cells, HepG2 (88065) and Huh7 (60104) cells were purchased from the Korean Cell Line Bank (KCLB, Seoul, Republic of Korea). HepG2 cells were maintained in Eagle's minimum essential medium (MEM) containing 10% fetal bovine serum (FBS), 100 U/ml penicillin/streptomycin (PS), and 25 mM N-2 hydroxyethylpiperazine-N-2-ethane sulfonic acid (HEPES). Huh-7 cells were maintained in RPMI-1640 medium containing 10% FBS and 100 U/ml PS. HepG2-hNTCP-C4 cells were kindly gifted by Dr. Koichi Watashi from National Institute of Infectious Disease (Tokyo, Japan). HepG2-hNTCP-C4 cells were maintained in DMEM/F-12 supplemented with GlutaMAX, 10% FBS, 100 U/ml PS, 10 mM HEPES, 5 µg/ml insulin, and 500 µg/ml G418. HepaRG cells (HPR116) were purchased from Biopredic international (Saint-Gregoire, France) and were maintained in basal hepatic cell medium (MIL600C, Biopredic, Saint-Gregoire, France) with additives for maintenance/metabolism HepaRG medium (ADD620C, Biopredic, Saint-Gregoire, France).

In vivo assay and hydrodynamic injection

C57BL/6 mice (7-week-old males) were hydrodynamically injected in the tail vein with 10 µg of pHBV-1.2x-rt269L (WT, GenBank accession No. AY641558) or pHBV-1.2x-rt269I (generated by site-directed mutagenesis) plasmids carrying the full-length HBV genotype C genome in a volume of saline, which was equivalent to 10% of the mouse body weight. The total volume was delivered within 5-8 seconds. The mice were sacrificed 4 days after HBV-encoding DNA injection, and liver and serum were collected for analysis. All animal experiments were approved by the Institutional Animal Care and Use Committee (IACUC) of Seoul National University College of Medicine (SNU-210301-1-1).

Patients, HBV DNA extraction, and PCR amplification of the polymerase RT region

For this study, serum samples were collected from 90 (KU) or 97 (SNU3) patients with CHB, all patients were diagnosed with chronic hepatitis B and confirmed that no treatment such as nucleos(t)ide analogs (NAs) or interferon was initiated (Table 3-4). These selection criteria include HBVs antigen (HBsAg) positive results for more than 6 months and detection of HBV-DNA virus. It was excluded in the case of hepatitis C infection or co-

infection of acquired immune syndrome (HIV), autoimmune liver disease, alcohol or drug addiction. Serum was stored at -80 degrees and used in this study. Viral DNA extracted from serum was stored at -20 degrees and used for experiments. To determine the correlation between the polymorphism at the 269th amino acid and characteristics of disease, clinical factors and polymerase RT regions were assessed. This report was approved by the Institutional Review Board of Konkuk University Hospital (KUH-1010544) and Seoul National University Hospital (1012-131-346 and 1808-067-965). For this cohort study, HBV DNA was extracted from the serum of patients using a QIAamp DNA Blood Mini kit (QIAGEN, Hilden, Germany), and the sample was dissolved in Tris-EDTA buffer (10 mM Tris-HCl and 1 mM ethylenediaminetetraacetic acid, pH 8.0). First-round PCR was performed using primers POL-RT1 and the amplicon was used as a template for second-round PCR using primers POL-RT2 (Table 1). The PCR products were subjected to direct sequencing analysis.

HBV DNA extraction and PCR amplification of the polymerase RT region

For this cohort study, HBV DNA was extracted from the serum of patients using a QIAamp DNA Blood Mini kit (QIAGEN, Hilden, Germany), and

the sample was dissolved in Tris-EDTA buffer (10 mM Tris-HCl and 1 mM ethylenediaminetetraacetic acid, pH 8.0). First-round PCR was performed using primers POL-RT1 and the amplicon was used as a template for second-round PCR using primers POL-RT2 (Table 1). The PCR products were subjected to direct sequencing analysis.

HBV genotyping

A total of 1,032-bp polymerase RT sequences were examined by direct sequencing and compared to the sequences of the reference strains representing each of the genotype (A-H including the C strains) obtained from GenBank. The sequences of the RT region were compared via the Bayesian method in the phylogenetic/molecular evolutionary analysis with MrBayes version 3.2.7, and the phylogenetic tree was constructed using FigTree version 1.4.3. The maximum-likelihood method was also used for the phylogenetic analysis with MEGA version 10.0. Phylogenetic trees were reconstructed using 1,000 bootstrap replicates, and the mean genetic distances were estimated using the Kimura two-parameter with invariant sites and gamma model.

Plasmid and site-directed mutagenesis

pHBV-1.2x (GenBank accession No. AY641558) containing the full-length HBV genotype C genome was used for site-directed mutagenesis to generate polymerase RT mutant DNA constructs with an i-pfu kit (iNtRON, Seongnam, Republic of Korea). Mutagenesis was performed using the primer rt269I based on the rt269L construct. To exclude the CMV promoter, HBV full-genome constructs were cut by the restriction enzyme *Sma*I and prepared for linear genome formation.

Transfection

HepG2 human hepatocellular carcinoma cells and Huh7 cells purchased from the Korean Cell Line Bank (KCLB, Seoul, Republic of Korea) were grown at 37°C in a humidified environment containing 5% CO₂. pHBV-1.2x containing the full-length HBV genotype C genome (2.5 µg) was transiently transfected using Lipofectamine 3000 (Invitrogen, Carlsbad, CA, USA). To normalize the transfection efficacy data, pSV-β-galactosidase (0.25 µg) was cotransfected, and the enzyme assay was performed using a β-Galactosidase Enzyme Assay System with Reporter Lysis buffer (Promega, Madison, WI, USA) following the manufacturer's protocol.

Total RNA extraction and real-time polymerase chain reaction (RT-qPCR)

Total RNA was extracted from transfected cells or mouse liver tissue using TRIzol, and the target genes were amplified with SensiFAST SYBR Lo-ROX One-Step kits (BioLine, London, UK). The transcription level was analyzed using qRT-PCR with the primer sets shown in Table S1, and the housekeeping gene β -actin was used as the internal control.

Preparation of HBV from transiently transfected cells and infection assay

For the infection experiments, the supernatant of the culture medium of HepG2 cells transiently transfected with 1.2x-rt269L or rt269I HBV plasmids was collected. The supernatant was purified through a sterile 0.45- μ m pore size filter and precipitated with 6% polyethylene glycol (PEG) 8000 overnight. The medium was ultracentrifuged, and the collected pellet was resuspended in PBS containing 15–25% fetal calf serum (FCS). After quantification by qPCR, 3×10^9 HBV genome equivalents per milliliter were aliquoted and stored at -80°C . HepG2-hNTCP-C4 cells were seeded in 6-well plates. The infection assay was performed with concentrated virus in the presence of 4% PEG8000 at 37°C for 20 h. The HepG2-hNTCP-C4 cells

were kindly provided by Dr. Koichi Watashi (National Institute of Infectious Disease, Tokyo, Japan).

Immunofluorescence analysis

Cells were seeded and cultivated in two-chamber glass slides (Nunc, Roskilde, Denmark) for 12 h before each experiment. The cells were fixed with 4% paraformaldehyde (PFA) and permeabilized with 0.25% Triton-X 100 for 10 min. The cells were stained with primary antibodies (1:100, overnight at 4°C) and secondary antibodies (1:1000, 2 h at room temperature) in 1% bovine serum albumin (BSA) in PBST and mounted in mounting medium containing DAPI (VECTASHIELD, Vector Laboratories, Inc., Burlingame, CA, USA). Images were captured and analyzed using software to quantify the staining intensity (Leica Software analysis, LAS X and ImageJ program, version 1.52a).

Western blot analysis

The harvested cells were lysed with RIPA buffer (CST, 9806) containing protease and phosphatase inhibitors (Hoffmann-La Roche Inc., Basel, Switzerland) and incubated for 20 min on ice. The lysed cells were centrifuged for 30 min at 13,000 rpm, and the lysates were collected for

Western blotting. Protein samples were separated by electrophoresis, transferred to nitrocellulose membranes, and blocked for 1 h with 5% skim milk or BSA. The membranes were incubated overnight at 4°C with the primary antibodies (1:1000). The next day, the membranes were washed with 0.1% Tween-20 in Tris-buffered saline and incubated with horseradish peroxidase-conjugated secondary antibodies (1:10000) for 2 h. After the ECL solution was applied to the membrane, proteins were detected on an imager (AI680).

Mitochondrial membrane potential ($\Delta\Psi_m$) assay

JC-1 staining

To determine the $\Delta\Psi_m$, the dual emission potentiometric dye JC-1 was used. JC-1 aggregates fluoresce red (~ 597 nm), whereas monomers fluoresce green (~ 539 nm). The relative intensity of red and green fluorescence was used to indicate the variation in $\Delta\Psi_m$. Cells were incubated with 1 μ M JC-1 (MCE, Monmouth Junction NJ, USA). Images were acquired with an Olympus FV3000 confocal microscope (Olympus, Tokyo, Japan).

Tetramethylrhodamine methyl ester (TMRM) staining

Cells were incubated in medium containing 250 nM TMRM (Invitrogen) for 30 min at 37°C and 5% CO₂ in the dark. After staining, the cells were

washed three times with PBS and mounted in mounting medium containing DAPI (VECTASHIELD, Vector Laboratories, Inc., Burlingame, CA, USA). Images were captured using an Olympus FV3000 confocal microscope (Olympus, Tokyo, Japan).

Mitochondrial functionality assay

A 48-well culture plate was seeded with 1×10^6 cells. After washing with PBS, the cells were gently scraped from the plate with a cell scraper. The cells were added to a 96-well round-bottom plate. The cells were resuspended in a prewarmed antibody and probe mixture (MitoTracker Red and Green) and incubated for 15 min at 37°C. After staining, the cells were resuspended in PBS + 2% FCS for analysis by flow cytometry. Functional mitochondria fluoresce MitoTracker Green^{high} and MitoTracker Red^{high}, while dysfunctional mitochondria fluoresce MitoTracker Green^{high} and MitoTracker Red^{low} (1).

Immunohistochemistry (IHC)

The liver sections were fixed with 4% paraformaldehyde for 72 h in 4°C and embedded in paraffin. The embedded tissues were cut into 4 ~ 6- μ m-thick sections and deparaffinized with a xylene/ethanol solution. Antigen retrieval

was performed with the heat-mediated method (sodium citrate buffer), and endogenous peroxidase was blocked by 3% H₂O₂. For IHC staining, the sections were incubated with primary and secondary antibodies, and chromogenic detection was developed through the conversion of 3,3'-diaminobenzidine (DAB) to a brownish precipitate that remained permanently detectable on slides and were visualized by light microscopy.

Transmission electron microscopy (TEM)

The cells were fixed overnight in a mixture of cold 2.5% glutaraldehyde in 0.1 M phosphate buffer (pH 7.2), and 2% paraformaldehyde in 0.1 M phosphate (pH 7.2). These tissues were postfixed for 1.5 h in 2% osmium tetroxide in 0.1 M phosphate buffer at room temperature. The cells were then washed briefly with 0.1 M phosphate buffer, dehydrated through a graded 50, 60, 70, 80, 90, 95, and 100% ethanol (X2) series, infiltrated with a propylene oxide and EPON epoxy resin mixture (Embed 812, Nadic methyl anhydride, poly Bed 812, dodecenylsuccinic anhydride, dimethylaminomethyl phenol; Electron Microscopy Polysciences, and ultimately embedded with only epoxy resin. The epoxy-resin-mixed samples were loaded into capsules and polymerized at 80°C overnight. In preparation for light microscopy analysis, samples were cut into 1.0 nm sections and stained with 1% toluidine blue for 45 s on a hot plate at 80°C.

Thin sections were cut with an ultramicrotome (RMC MT-XL) and collected on a copper grid. Specifically, areas identified for thin sectioning were cut into 65 nm slices and stained with saturated 4% uranyl acetate and 4% lead citrate before examination with a transmission electron microscope (JEM-1400; Japan) at 80 Kv.

XBP1 splicing assay

An X-box-binding protein 1 (XBP1) fragment was PCR amplified from cDNA isolated from HBV-infected or thapsigargin-treated cells using the specific primers pXBP1F, 5'-GGATGCCTTAGTTACTGAAG-3', and pXBP1R, 5'-GTCCTTCTGGGTCGACTTCT-3'. The PCR amplicons were identified in a 3% agarose gel and visualized using a Gel Documentation System (Bio-Rad, CA, USA).

TUNEL assay

For TUNEL assays, tissue slides and cells were reacted with terminal deoxynucleotidyl transferase (TdT) enzyme and fluorescently labeled with 2'-deoxyuridine 5'-triphosphate (dUTP) at 37 °C for 1 h. The nuclei were stained with DAPI. TUNEL-positive cells were captured and analyzed using software to quantify the staining intensity (Leica Software analysis, LAS X and ImageJ program, version 1.52a).

8-OHdG ELISA Assay

Genomic DNA was extracted from transfected cells using a QIAamp Blood DNA extraction kit (QIAGEN, Hilden, Germany). For the detection of 8-hydroxy-2'-deoxyguanosine (8-OHdG) activity, a competitive ELISA was performed with an 8-OHdG analysis kit (OxiSelect Oxidative DNA Damage ELISA kit, Cell Biolabs, San Diego, CA, USA) according to the manufacturer's protocol.

Cytochrome c release, ATP production, and DNA fragmentation

Cytochrome c release (MCTC0, R&D Systems, Inc. Minneapolis, MN, USA), ATP production (ab83355, Abcam, Cambridge, UK), and DNA fragmentation (11774425001, Sigma–Aldrich, MO, USA) were determined according to the manufacturer's manual.

Statistical analysis

The experimental data were analyzed with GraphPad Prism 9 (GraphPad Software, La Jolla, CA, USA). All experiments were independently repeated three times, and statistical analysis results are indicated in the figure legends.

The ***p*** value indicating statistical significance was set at $*p < 0.05$; $**p < 0.01$; or $***p < 0.001$.

Table 1. PCR primers used in this study

Primer	Forward	Reverse
POL-RT1	CAG CCT ACT CCC ATC TCT CCA CCT CTA AG-3	GCT CCA GAC CGG CTG CGA GC-3
POL-RT2	CCT CAG GCC ATG CAG TGG AA	GTA TGG ATC GGC AGA GGA GC
rt269I-C	GAA CAT ATT GTA CAA AAA ATC AAG CAA TGT TTT CGG AAA	TTT CCG AAA ACA TTG CTT GAT TTT TTG TAC AAT ATG TTC
Human mitochondrial DNA 1	CATGCCCATCGTCCTAGAAT	ACGGGCCCTATTTCAAAAGAT
Human mitochondrial DNA 2	CCCTAACACCAGCCTAACCA	AA AGTGCATACCGCC7AAAAC
Human mitochondrial DNA 3	TCCAACCT CATGAGACCCACA	TGAGGCT TGGATTAGCGTTT
Human ATF4	GAC CGA AAT GAG CTT CCT GA	ACC CAT GAG GTT TGA AGT GC
Human ATF4	TCT CAT TCA GGC TTC TCA CGG CAT	AAG CTC ATT TCG GTC ATG TTG CGG
Human ATF6 EMDM1	TTC CCT CCT GGT GGA ATT TG	AGG CCA CTC TGC TTT CCA AC
Human XBP1s	TGC TGA GTC CGC AGC AGG TG	GCT GGC AGG CTC TGG GGA AG
Human Beclin 1	ACC GTG TCA CCA TCC AGG AA	GAA GCT GTT GGC ACT TTC TGT
Human LC3	GAG AAG CAG CTT CCT GTT CTG G	GTG TCC GTT CAC CAA CAG GAA G
Human NADH dehydrogenase	ATA CCC ATG GCC AAC CTC CT	GGG CCT TTG CGT AGT TGT AT
Human cytochrome c oxidase	ATG ACC CAC CAA TCA CAT GC	ATC ACA TGG CTA GGC CGG AG
β -Actin	ATT GCC GAC AGG ATG CAG AA	GCT GAT CCA CAT CTG CTG GAA

Table 2. List of Antibodies

Antibody Name	Company
Anti- GAPDH	Santa Cruz Biotechnology (Dallas, TX, USA), sc-25778 and sc-293335
Anti- PGC1 α	Santa Cruz Biotechnology (Dallas, TX, USA), sc-517380
Anti-PreS1(AP1)	Santa Cruz Biotechnology (Dallas, TX, USA), sc-57761
Anti- PERK	Cell Signaling Technology (Danvers, MA, USA), 3192
Anti- phospho-PERK	Cell Signaling Technology (Danvers, MA, USA), 3179 Invitrogen (Carlsbad, CA, USA), PA5-102853
Anti- ATF4	Cell Signaling Technology (Danvers, MA, USA), 11815
Anti-phospho-eIF2 α	Cell Signaling Technology (Danvers, MA, USA), 3597
Anti- IRE1 α	Cell Signaling Technology (Danvers, MA, USA), 3294
Anti- cleaved-caspase 3	Cell Signaling Technology (Danvers, MA, USA), 9661
anti- LC3B	Cell Signaling Technology (Danvers, MA, USA), 2775
Anti-CHOP	Cell Signaling Technology (Danvers, MA, USA), 2895
Anti-PI3KC3	Cell Signaling Technology (Danvers, MA, USA), 4263
Anti-PI3K	Cell Signaling Technology (Danvers, MA, USA), 4228
Anti-phosphoAkt	Cell Signaling Technology (Danvers, MA, USA), 9271
Anti-ATF6	Proteintech Group, Inc (Rosemont, IL, USA), 24169-1-AP
Anti-Beclin 1	Abcam (Cambridge, UK), ab62557
Anti-mTOR (phospho)	Abcam (Cambridge, UK), ab109268
Anti-PINK1	Abcam (Cambridge, UK), ab23707
Anti-Parkin	Abcam (Cambridge, UK), ab77924
Anti-phospho-IRE1 α	Abcam (Cambridge, UK), ab48187 Invitrogen (Carlsbad, CA, USA), PA1-16927
Anti-Flag M2 antibody	Sigma–Aldrich (St. Louis, MO, USA), F1804
Alexa Fluor 488-conjugated goat anti-rabbit IgG (H+L)	Invitrogen (Carlsbad, CA, USA), A-11008
Alexa Fluor 594-conjugated goat	Invitrogen (Carlsbad, CA, USA),

anti-mouse IgG (H+L)	A-11005
MitoSOX Red mitochondrial superoxide indicator	Invitrogen (Carlsbad, CA, USA), <u>M36008</u>
MitoTracker, Deep Red FM	Invitrogen (Carlsbad, CA, USA), M22426,
MitoTracker, Green FM	Invitrogen (Carlsbad, CA, USA), M7514
Tunel apoptosis detection kit (DNA fragmentation/fluorescence staining)	Millipore, (Billerica, MA, USA), 17-141
Bafilomycin-A1	Sigma–Aldrich (St. Louis, MO, USA), B 1793

Results

rt269L leads to improved mitochondrial maintenance with increased functional mitochondria and bioenergetics

Previously, I reported that the rt269I HBV variant versus rt269L led to liver disease progression, as indicated by enhanced mitochondrial stress and reactive oxygen species (ROS) production levels [17]. Therefore, in this study, I investigated mitochondrial features and their functionality in two types of HBV genotype C2 infection. First, the mitochondrial membrane potential ($\Delta\Psi_m$) was measured by JC-1 staining, a potential-sensitive fluorescent dye. As shown in Fig. 1A, rt269L infection led to greater emission of red fluorescence and lower emission of green fluorescence compared to rt269I. In addition, TMRM, another cell-permeant dye that accumulates in active mitochondria with intact membranes, was also more intense in the mitochondria of rt269L-infected cells than in rt269I-infected cells (Fig. 1B, Fig. 2). Then, I analyzed the mitochondrial functionality in cells infected with each HBV type by flow cytometry based on mitochondrial mass (green fluorescence) and membrane potential (red fluorescence).

The data revealed that rt269L-infected cells contained a higher percentage of functional mitochondria (Green^{high} and Red^{high}) and a lower percentage of dysfunctional mitochondria (Green^{high} and Red^{low}) than rt269I-infected cells (Fig. 1C).

Next, intracellular mitochondrial biogenesis in HepG2-NTCP-C4 cells infected with rt269L or rt269I HBV virions was assessed by transmission electron microscopy (TEM). As shown in Fig. 3A, rt269L-infected cells contained increased numbers of mitochondria compared to rt269I-infected cells. mtDNA copy number is closely associated with cellular energy production [19], and PGC-1 α is known to promote ATP

production and energy homeostasis [20]. The data indicated that rt269L induced increased mtDNA gene transcription as well as increased PGC-1 α protein expression (Fig. 4). Consistently, rt269L infection enhanced ATP production in HepG2 cells and liver tissues of the model mice (Fig. 3B). Moreover, the mitochondrial cristae structures differed in mouse livers infected with rt269L or rt269I HBV. As shown in Fig. 3C, the liver tissue in mice injected with rt269L HBV contained mitochondria with normal and dense cristae structures. However, tissue exposed to rt269I HBV infection showed loss of normal cristae and many hollow areas, suggesting critically damaged inner mitochondrial matrices. Taken together, these results suggest that rt269L infection showed improved mitochondrial functionality with increased mitochondrial biogenesis and bioenergetics, while the rt269I variant led to impaired mitochondrial functionality.

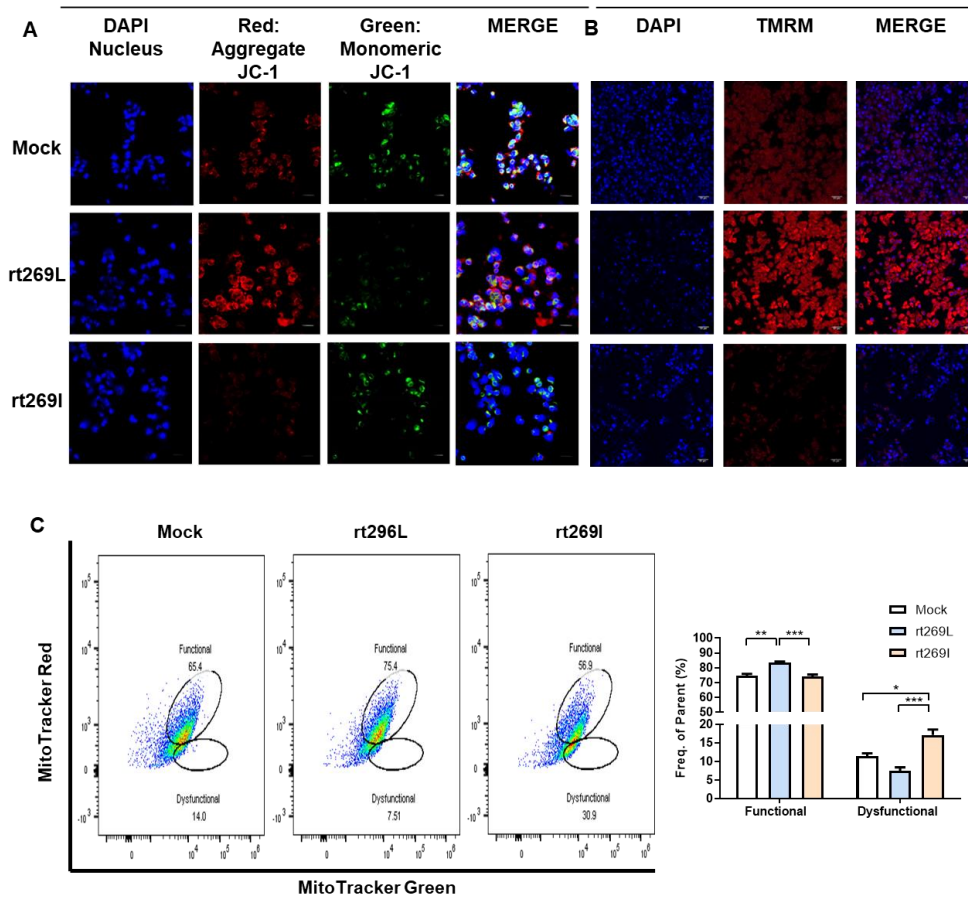


Fig. 1 **rt269L-infected cells showed improved mitochondrial maintenance with a high rate of functional mitochondria and biogenesis** **A, B** Confocal microscopy images showing HepG2 cells transfected with mock, rt269L, or rt269I HBV followed by JC-1 staining and TMRM staining indicating mitochondrial outer membrane permeabilization (MOMP) and $\Delta\Psi_m$. Nuclei were stained with DAPI (blue). Scale bar = 50 μm . **C** Evaluation of mitochondrial function by flow cytometry. Error shows the means \pm SEMs $*p < 0.05$, $**p < 0.01$, $***p < 0.001$.

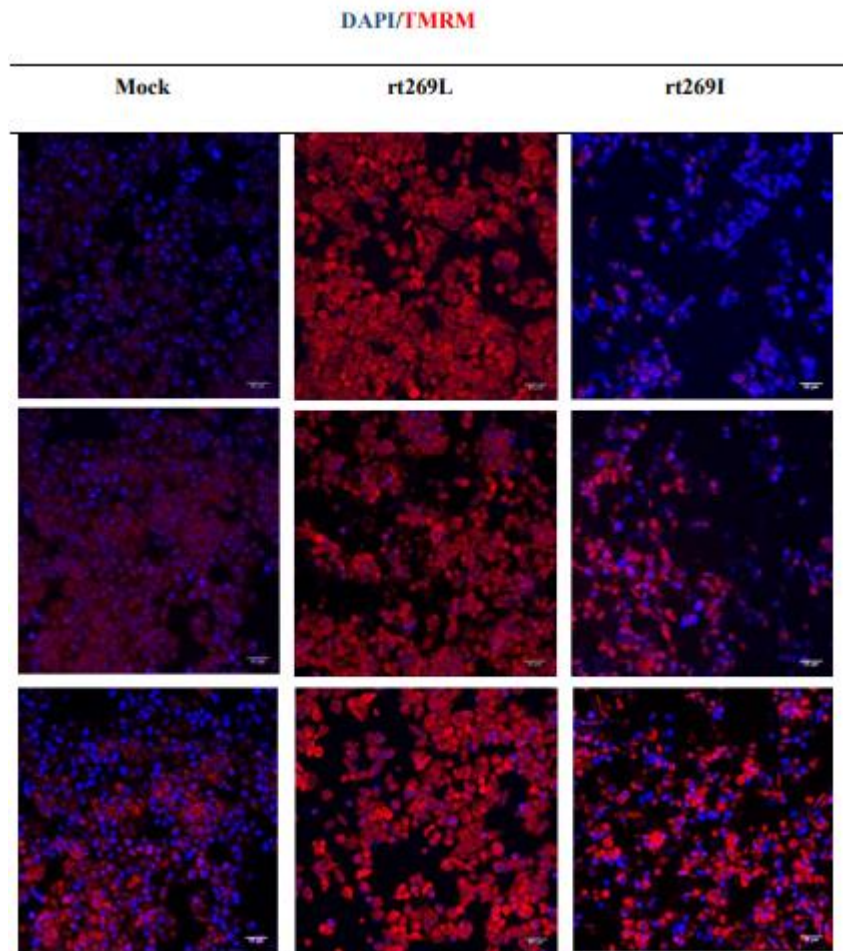


Fig. 2 Confocal microscopy images showing HepG2 cells transfected with mock, rt269L, or rt269I HBV followed TMRM staining indicating mitochondrial outer membrane permeabilization (MOMP) and $\Delta\Psi_m$. rt269L type showed improved mitochondrial maintenance with high rate of functional mitochondria and biogenesis. Confocal microscopy images showing HepG2 cells transfected with mock, rt269L, or rt269I HBV followed by TMRM staining. Mitochondrial outer membrane permeabilization (MOMP) and $\Delta\Psi_m$ were observed. Nuclei were stained with DAPI (blue). Scale bar = 50 μm .

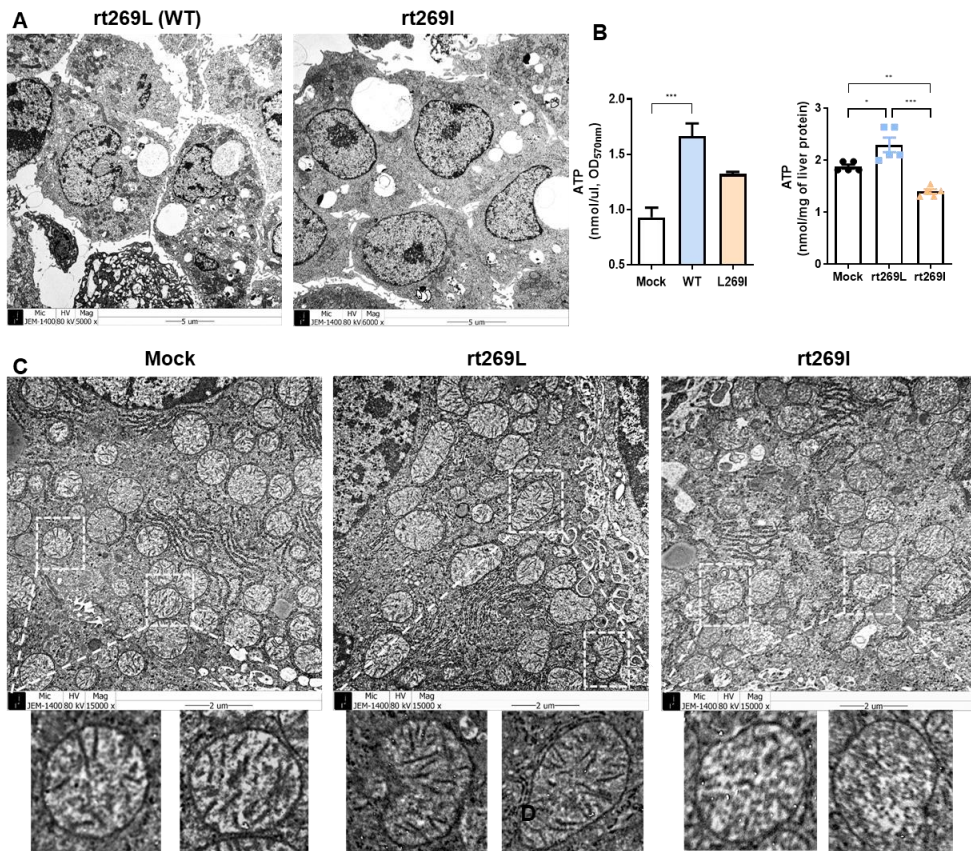


Fig. 3 **rt269L-infected cells showed improved mitochondrial bioenergetics with a high rate of functional mitochondria and biogenesis** **A** High magnification of mitochondria in rt269L- and rt269I-infected HepG2-NTCP-C4 cells (scale bars, 5 or 1 μm). **B** Mitochondrial ATP generation in HepG2 cells transfected with mock, rt269L, or rt269I vector or in liver tissues of mice hydrodynamically injected with mock, rt269L, or rt269I vector. **C** Mitochondrial cristae morphology and density in liver tissues of mice hydrodynamically injected with mock, rt269L, or rt269I HBV, assayed by TEM. Scale bar = 2 μm . The results were evaluated for statistical significance by one-way ANOVA with Tukey's post hoc test.

Differences were considered significant when $*p < 0.05$, $**p < 0.01$, and $***p < 0.001$.

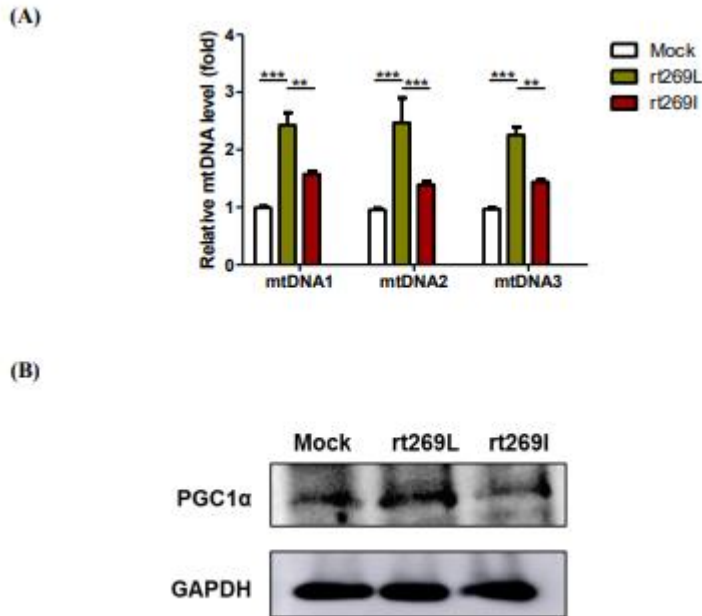


Fig. 4 **rt269L induced increased mtDNA gene transcription as well as increased PGC-1 α protein expression** (A) WT (rt269L) HBV induced higher transcription of three different mtDNA genes than rt269I HBV infection Mitochondrial copy numbers were calculated based on RT-qPCR results obtained with three different mtDNA primer sets. The results were evaluated for statistical significance by one-way ANOVA with Tukey's post-hoc test or t-test. Differences were considered significant when $*p < 0.05$, $**p < 0.01$, or $***p < 0.001$. (B) Protein expression levels were analyzed by Western blotting with antibodies against PGC1 α and GAPDH. The relative intensity compared to GAPDH was analyzed. $*p < 0.05$, $**p < 0.01$, $***p < 0.001$

rt269L activates PERK-p-eIF2 α -ATF4 signaling

Mitochondrial functionality is closely related to cellular signals, including ER stress signals [21]. As I verified a significant difference in mitochondrial functionality between rt269L and rt269I HBV infection, I investigated whether the ER stress induction levels differed. First, I compared the expression levels of three UPR-related proteins, PERK, IRE1 α , and ATF6, in three different hepatocytes, Huh7, HepG2, and HepG2-NTCP-C4 cells. As shown in Fig. 5A, rt269L HBV mainly induced PERK signaling, and the protein expression levels of p-PERK and p-eIF2 α were significantly increased in rt269L-infected cells. The immunofluorescence data also revealed that rt269L-infected cells increased p-eIF2 α -positive signals (Fig. 5B). A similar result was obtained in the liver tissue of mice hydrodynamically infected with rt269L HBV, as indicated via immunohistochemistry (IHC) staining (Fig. 5C, Fig. 6). Moreover, the ATF4 expression level was highly enhanced in rt269L-infected cells (Fig. 7A), indicating that rt269L induced PERK-eIF2- α -ATF4 axis activation. As ATF4 is considered a key stress regulator [22], I further investigated the signal in genotype A HBV infection. To verify this, I used a plasmid and pHY92 vector containing a copy of the 1.1x-unit length HBV genome (genotype A HBV strain identical to GenBank AF305422) and performed a site-directed mutagenesis assay. Interestingly, enhanced ATF4 expression was observed

in rt269L-infected cells in both genotypes A and C (Fig. 7B), which indicates that the HBV pol rt269L region is associated with PERK-eIF2- α -ATF4 axis activation. Meanwhile, an XBP1 splicing assay was performed, and neither rt269L nor rt269I HBV induced IRE1 α -sXBP signaling, but only thapsigargin (Tg) led to XBP splicing, showing spliced (269 bp) and unspliced (295 bp) forms (Fig. 7C). In addition, SYBR-based quantitative RT-PCR was performed, and the ATF4-encoding gene was profoundly upregulated in rt269L-infected cells, but no change was observed in the ATF6 and XBP1 genes (Fig. 7D). Altogether, rt269L type activated the PERK-eIF2 α -ATF4 pathway, but rt269I type failed to induce the UPR under cellular stress in the *in vitro* or *in vivo* assays.

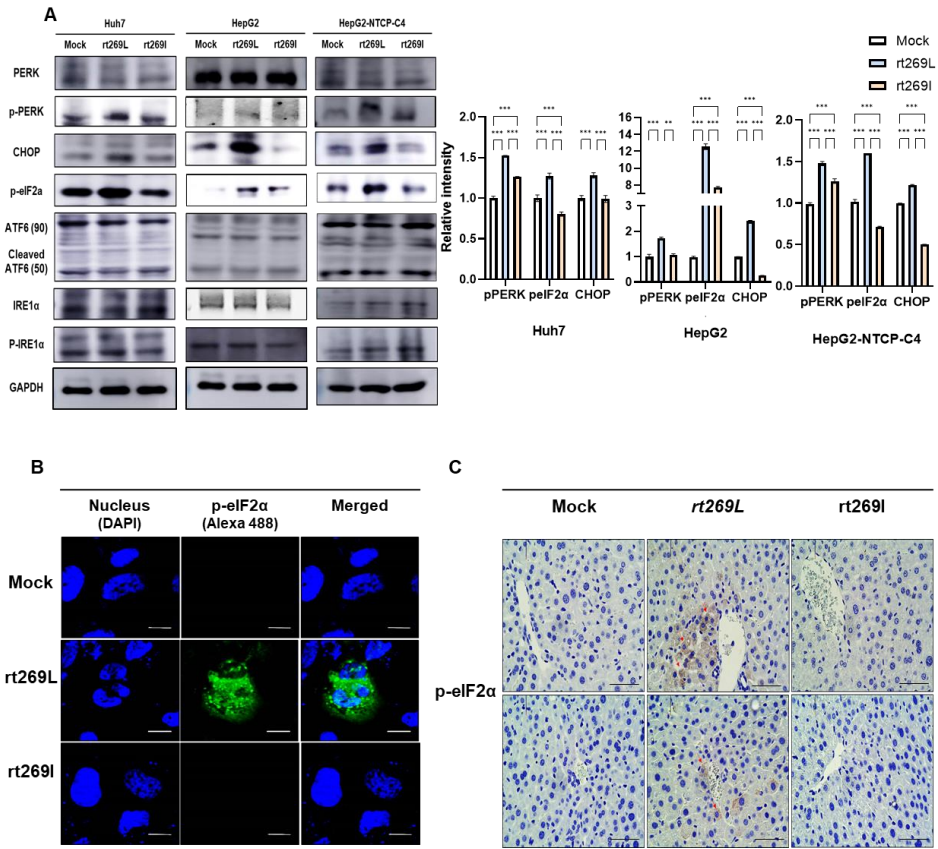


Fig. 5 *rt269L* activates the PERK-mediated UPR pathway, but an impaired UPR is shown in *rt269I*-infected cells. **A** Markers of ER stress in Huh7, HepG2, and HepG2-NTCP-C4 cells as measured by Western blotting after transfection or infection with mock, *rt269L*, or *rt269I* HBV. Some blots were cropped to improve the clarity and conciseness of the presentation. **B** Phosphorylation of eIF2 α determined by immunofluorescence. HepG2 cells were transfected with a mock, *rt269L*, or *rt269I* vector and then immunostained with antibodies and DAPI stained and viewed by confocal microscopy. Scale bar = 10 μ m. **C** Immunohistochemical analysis of p-eIF2 α expression (red arrow) in paraffin-embedded liver tissues (magnification 100x, scale bar = 100 μ m, n=5 per group).

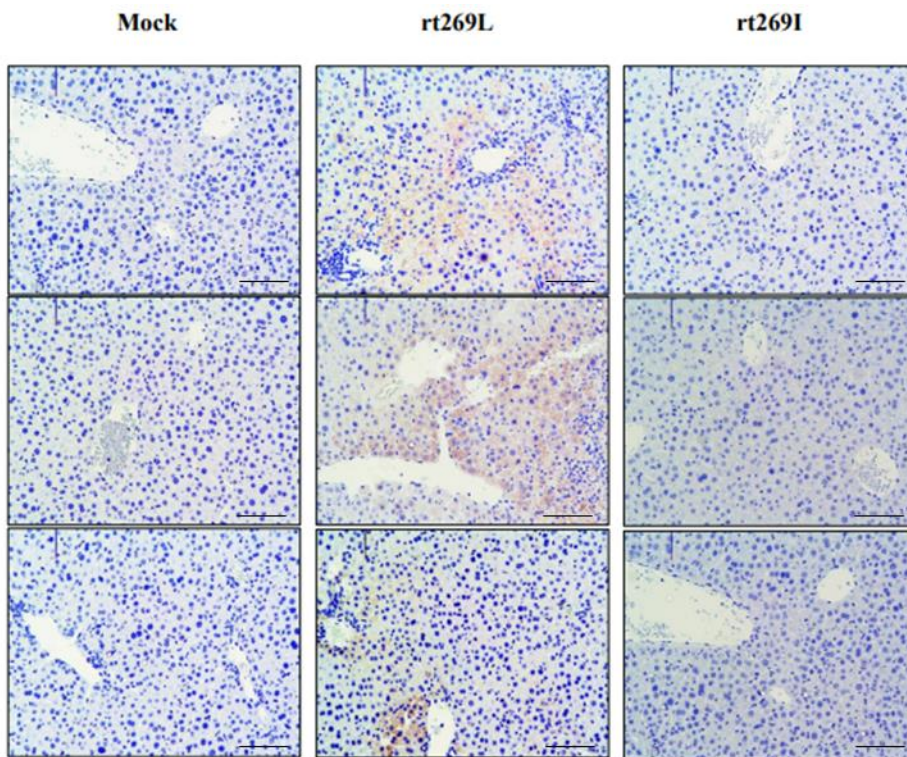


Fig. 6 Immunohistochemical analysis of p-eIF2 α expression (red arrow) in paraffin-embedded liver tissues WT (rt269L) HBV induces ER stress and activates the PERK-mediated pathway in the unfolded protein response (UPR) Immunohistochemical analysis of p-eIF2 α expression in paraffin-embedded liver tissues (magnification 100x, scale bar = 100 μ m, n=5 per group)

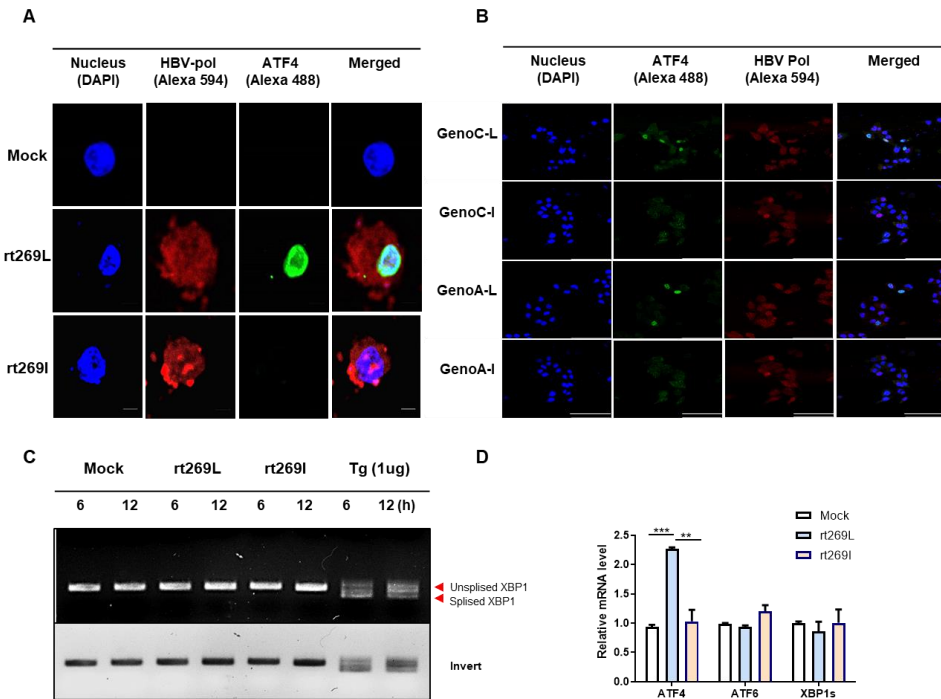


Fig. 7 *rt269L* activates PERK-peIF2 α -ATF4 signaling **A, B** ATF4 and HBV polymerase expression determined by immunofluorescence. Scale bar = 10 μ m **C** Agarose gel (3%) electrophoresis of XBP1 fragments (unspliced, 295 bp; spliced, 269 bp) from RNA isolation from HepG2 cells transfected with mock, *rt269L*, or *rt269I* HBV or treated with thapsigargin (Tg, 1 μ g/ml) for 6 and 12 h. **D** RT-qPCR analysis of the transcription levels of UPR- and ER stress-related genes 10 h posttransfection. Bar graph representing the relative expression levels (fold) of ATF4, ATF6, and sXBP1 calculated by the $2^{-\Delta\Delta C_t}$ method using β -actin as an endogenous control. ** p < 0.01, *** p < 0.001.

rt269L genotype C HBV infection led to enhanced autophagy induction

ER stress can activate autophagy gene transcription through the PERK-eIF2 α -ATF4 axis, and ATF4-mediated autophagy is known to be a potent cell survival mechanism [23, 24]. Because the rt269L type triggered PERK-eIF2 α -ATF4 signaling, I investigated autophagy induction signals. First, I immunostained endogenous LC3 protein with an anti-LC3 antibody. As shown in Fig. 8A, rt269L infection exhibited a higher immunoreaction with anti-LC3 Ab than rt269I infection. Then, I quantified EGFP-LC3-labeled autophagosomes in the absence or presence of the lysosome inhibitor bafilomycin A1. As shown in Fig. 8B, rt269L led to increased LC3 puncta in a basal state, and bafilomycin A1 significantly enhanced the accumulation of EGFP-LC3 puncta. In contrast, rt269I infection showed low LC3 puncta formation in the basal state, and the number of puncta was not increased with bafilomycin A1. Next, I investigated whether autophagy induction depends on PERK signaling using a PERK inhibitor (GSK2656157). As I expected, PERK inhibitor treatment dramatically reduced the LC3 puncta count compared to that in rt269L-infected cells, suggesting that PERK signaling is a key mediator of autophagy induction in rt269L-infected cells (Fig. 8C). The flow cytometry data consistently showed high autophagy induction in rt269L-infected cells (Fig. 9A and Fig. 10), and immunoblot data indicated higher LC3-II and Beclin 1 protein expression in rt269L-

infected cells than in rt269I-infected cells (Fig. 9B and Fig. 11). Furthermore, HepG2-NTCP-C4 cells infected with rt269L HBV virions formed many more autophagosomes and autolysosomes than rt269I-infected cells, as indicated by TEM (Fig. 9C). The mRNA expression of the autophagy markers Beclin 1 and LC3 was also detected by RT-qPCR, and the rt269L-infected cells showed higher autophagy gene transcription than the rt269I-infected cells (Fig. 9D).

Next, I compared the autophagy induction patterns in genotypes A and C (Fig. 12A-B). Interestingly, genotype A rt269L, generated by site-directed mutagenesis, showed enhanced autophagy induction, suggesting that polymerase with rt269L distinct in genotype C infection could play a key role in PERK-eIF2 α -ATF4 axis-mediated autophagy induction. Furthermore, I observed that HBx in rt269L strongly bound to PI3KC3, which induces autophagosome formation via PI3KC3/Beclin-2 activation [25, 26], in the immunoprecipitation assay (Fig. 13). Together, these data suggest that rt269L HBV infection significantly induces autophagy mainly by activating PERK signaling, while rt269I HBV infection fails to activate autophagy.

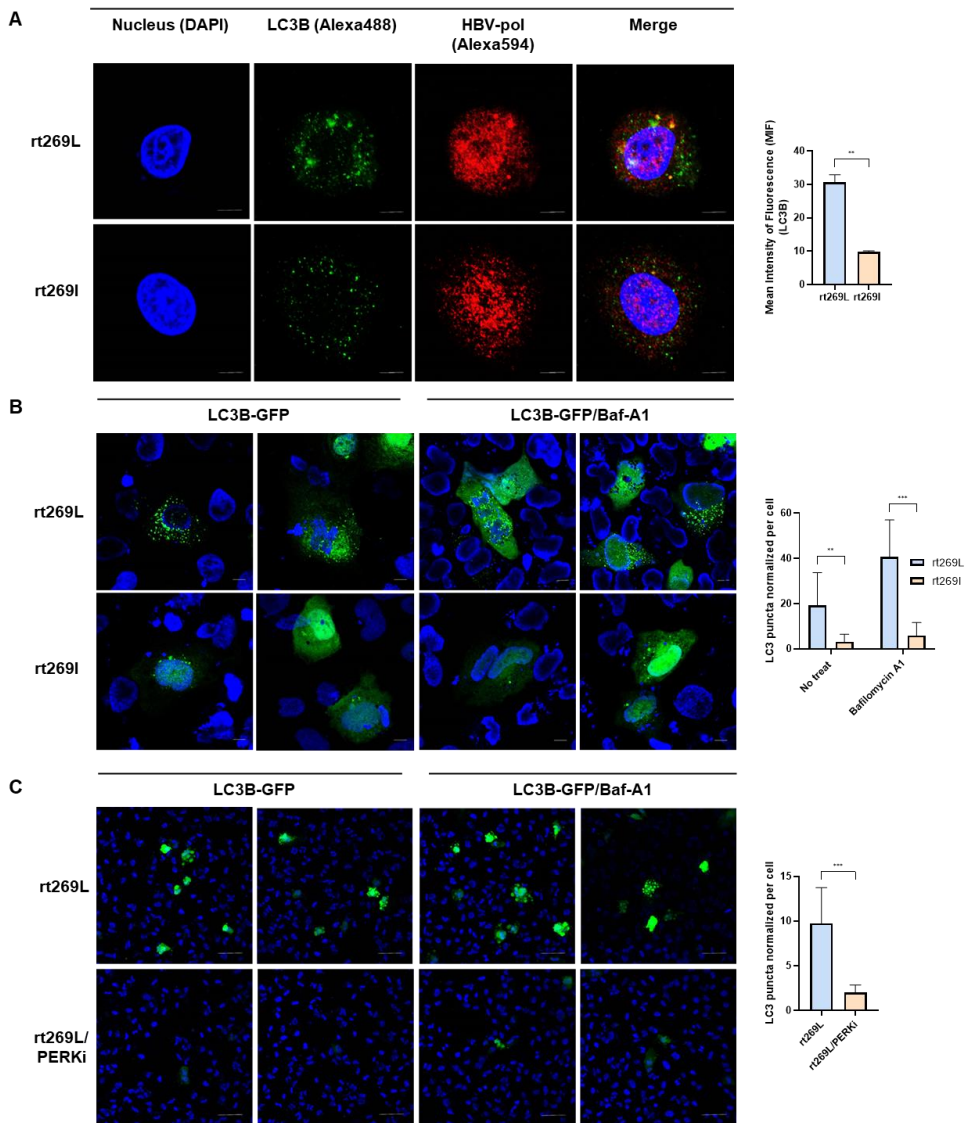


Fig. 8 rt269L genotype C HBV infection led to enhanced autophagy induction **A, B** Detection of autophagy induction by fluorescence microscopy. **A** HepG2 cells were transfected with the rt269L or rt269I vector. Cells were immunostained with antibodies against LC3B (green, Alexa 488) and HBV-pol (red, Alexa 594). The mean intensity of fluorescence (MIF) was analyzed. Scale bar = 10 μ m **B** Detection of LC3

puncta after transfection of the EGFP-LC3 vector. LC3 is recruited to autophagosomes, forming a punctate structure, as shown by green dots. The LC3-positive puncta in rt269L- or rt269I-transfected cells were analyzed in the absence or presence of bafilomycin A1 or a PERK inhibitor (GSK2656157, 10 μ M).

* $p < 0.05$, ** $p < 0.01$, *** $p < 0.001$.

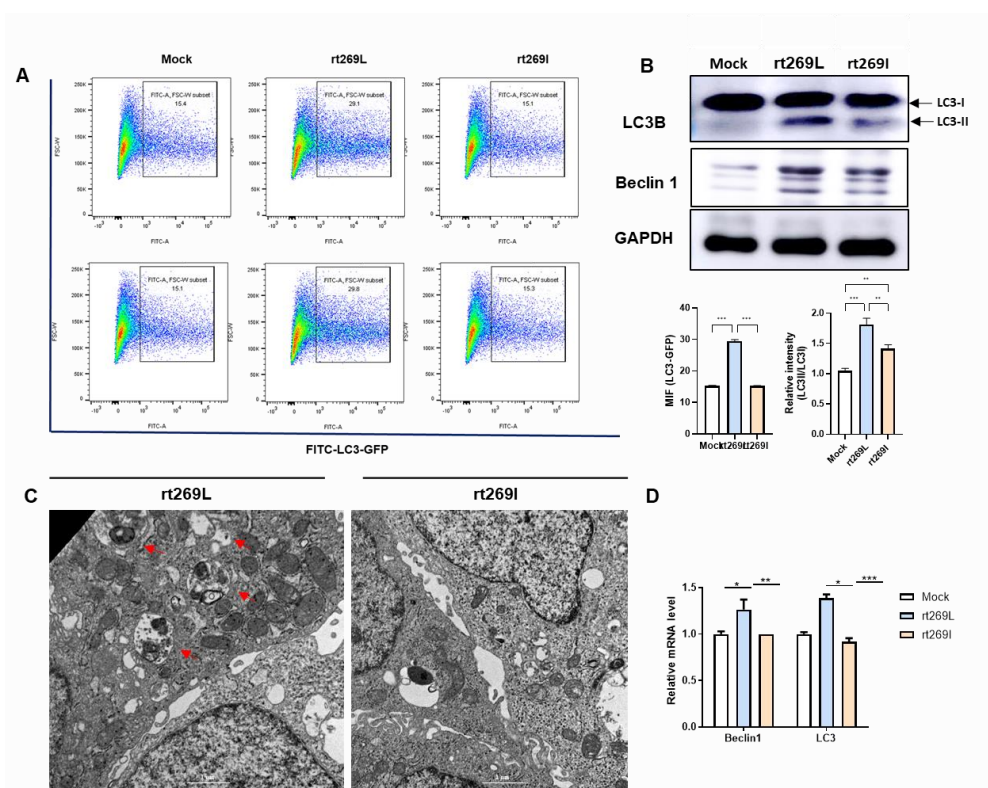


Fig. 9 rt269L genotype C HBV infection led to enhanced autophagy induction **A** EGFP-LC3 assay by flow cytometry. EGFP-LC3B-positive HepG2 cells cotransfected with mock, rt269L, or rt269I vectors were detected by flow cytometry. **B** Western blot analysis of the autophagy marker proteins LC3 and Beclin 1. The relative intensity of LC3II/LC3I staining was analyzed. $**p < 0.01$, $***p < 0.001$. **C** Detection of autophagosomes and autolysosomes in HepG2-NTCP-C4 cells infected with rt269L or rt269I HBV virions, assessed by TEM. The arrow denotes autophagic vacuoles. Scale bar: 1 μ m. **D** RT-qPCR analysis of Beclin1 and LC3 mRNA 10 h after HepG2-NTCP-C4 cell infection with PBS (Con), rt269L or rt269I HBV virions. $*p < 0.05$, $**p < 0.01$, $***p < 0.001$.

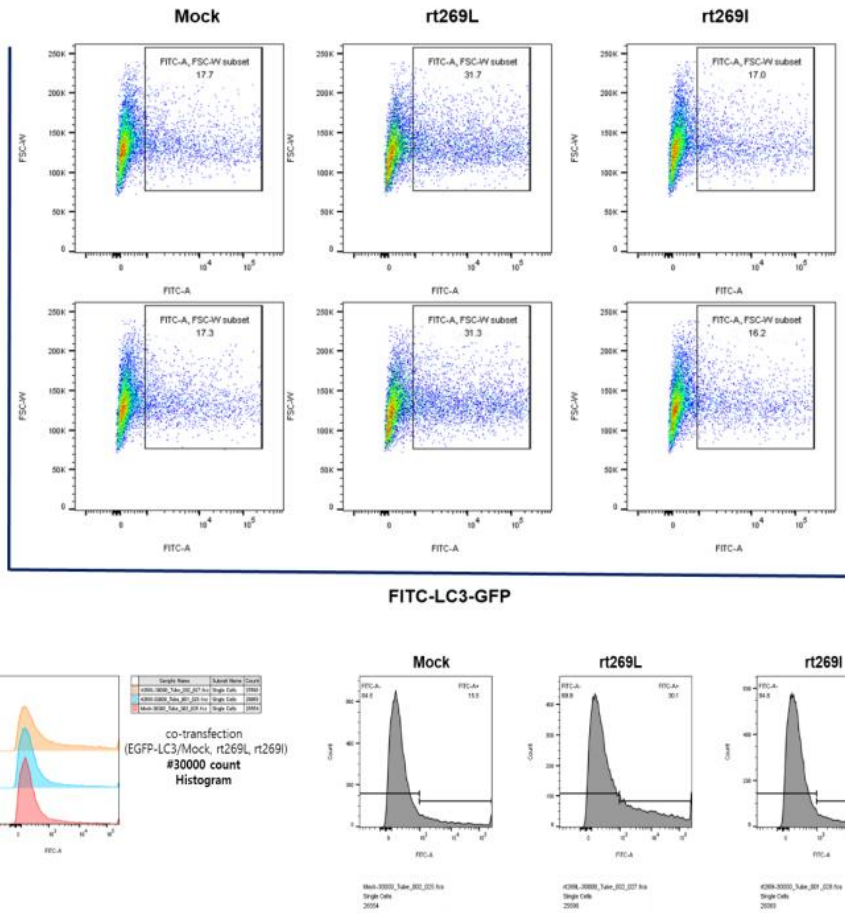


Fig. 10 EGFP-LC3 assay with flow cytometry EGFP-LC3B-positive HepG2 cells cotransfected with mock, rt269L, or rt269I HBV were detected by flow cytometry.

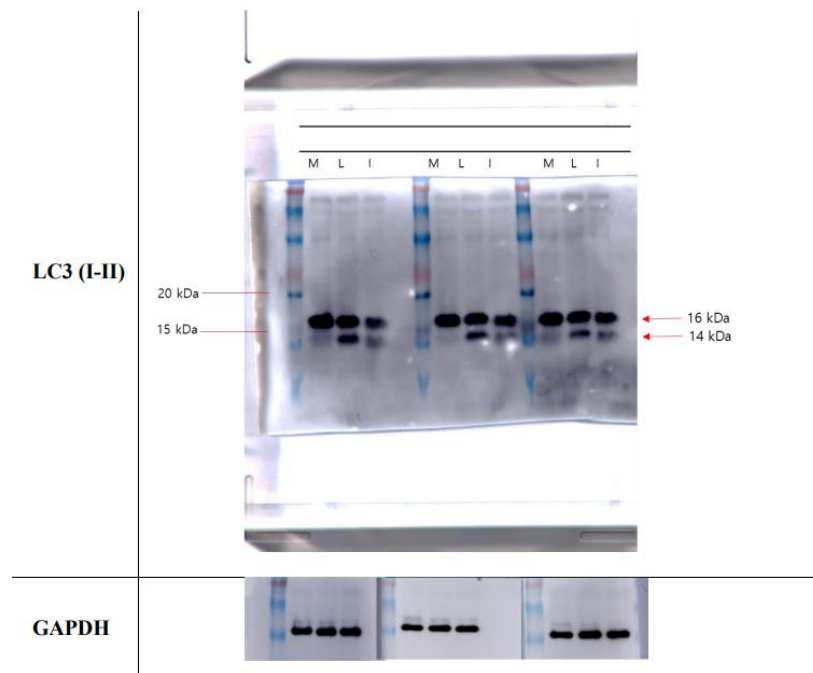


Fig. 11 Enhanced autophagy in rt269L HBV infection Western blots showing the autophagy marker protein LC3.

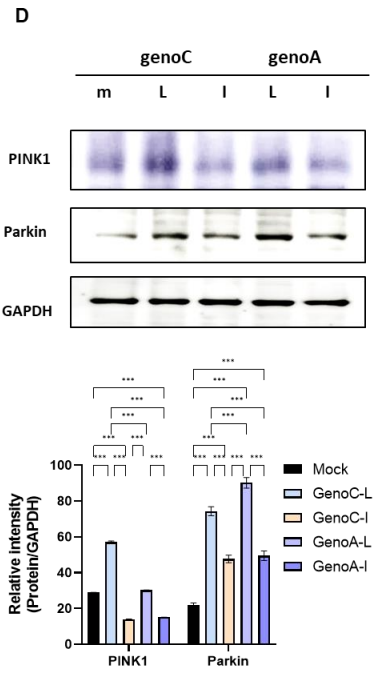
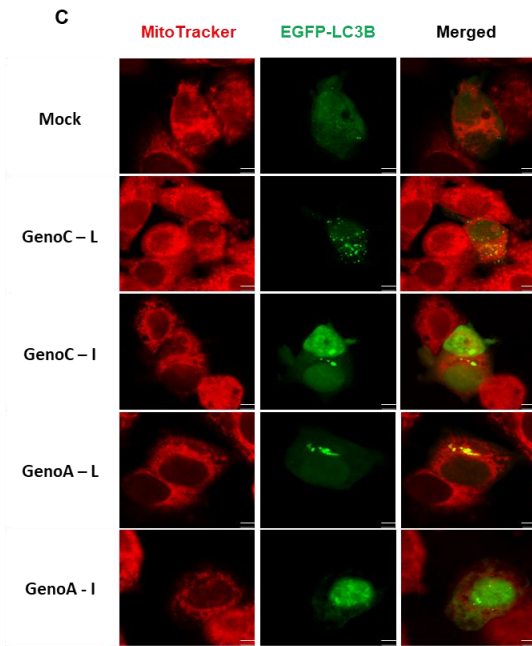
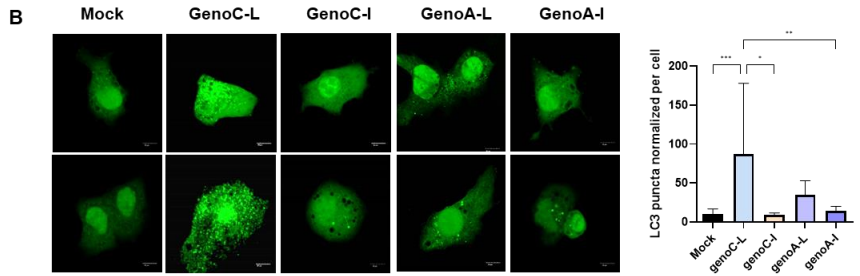
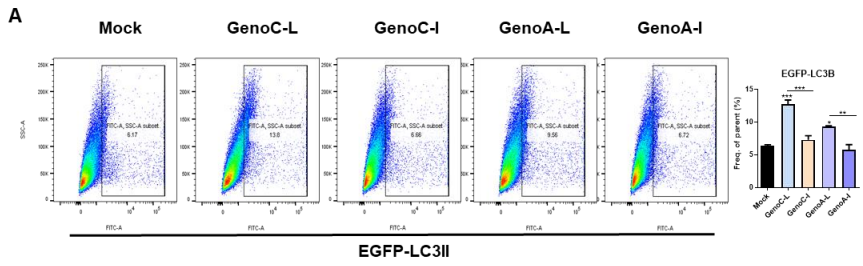


Fig. 12 Comparison of autophagy/mitophagy induction in genotype A and C HBV infection

A EGFP-LC3 assay by flow cytometry. EGFP-LC3B-positive HepG2 cells cotransfected with mock, rt269L (genotype A or C), or rt269I (genotype A or C) vectors were detected by flow cytometry.

B Detection of LC3 puncta after transfection of the EGFP-LC3 vector with genotype A or C vectors. LC3 is recruited to autophagosomes, forming a punctate structure, as shown by green dots.

C Immunofluorescence for the colocalization of autophagosomes with mitochondria. The EGFP-LC3-expressing vector was cotransfected with HBV genome plasmids. Mitochondria were stained with MitoTracker deep red, and yellow dots represent colocalized EGFP-LC3-positive autophagosomes with red-labeled mitochondria.

D Western blot analysis of the mitophagy marker protein PINK1. The relative intensity of PINK1/GAPDH staining was analyzed. ** $p < 0.01$, *** $p < 0.001$.

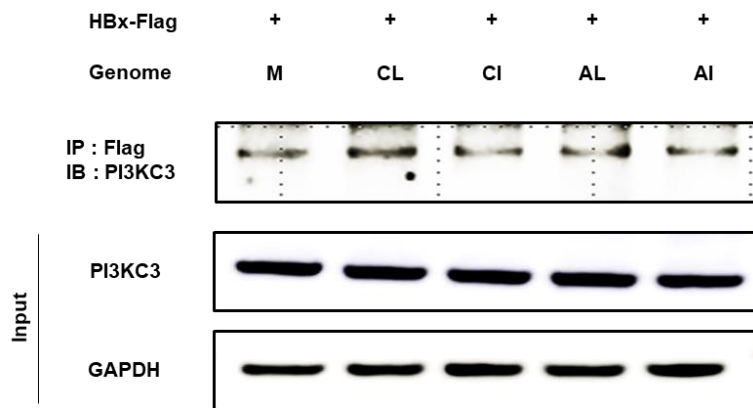


Fig. 13 HBx in rt269L strongly interact with PI3KC3 (VPS34) HBx-flag plasmid was cotransfected with Mock, GenoC-L, genoC-I, genoA-L, or genoC-I plasmid in HepG2 cells, as indicated. At 42 h post-transfection, cells were extracted and the cell lysates were subjected to IP with anti-Flag Ab followed by IB using anti-PI3KC3 Ab.

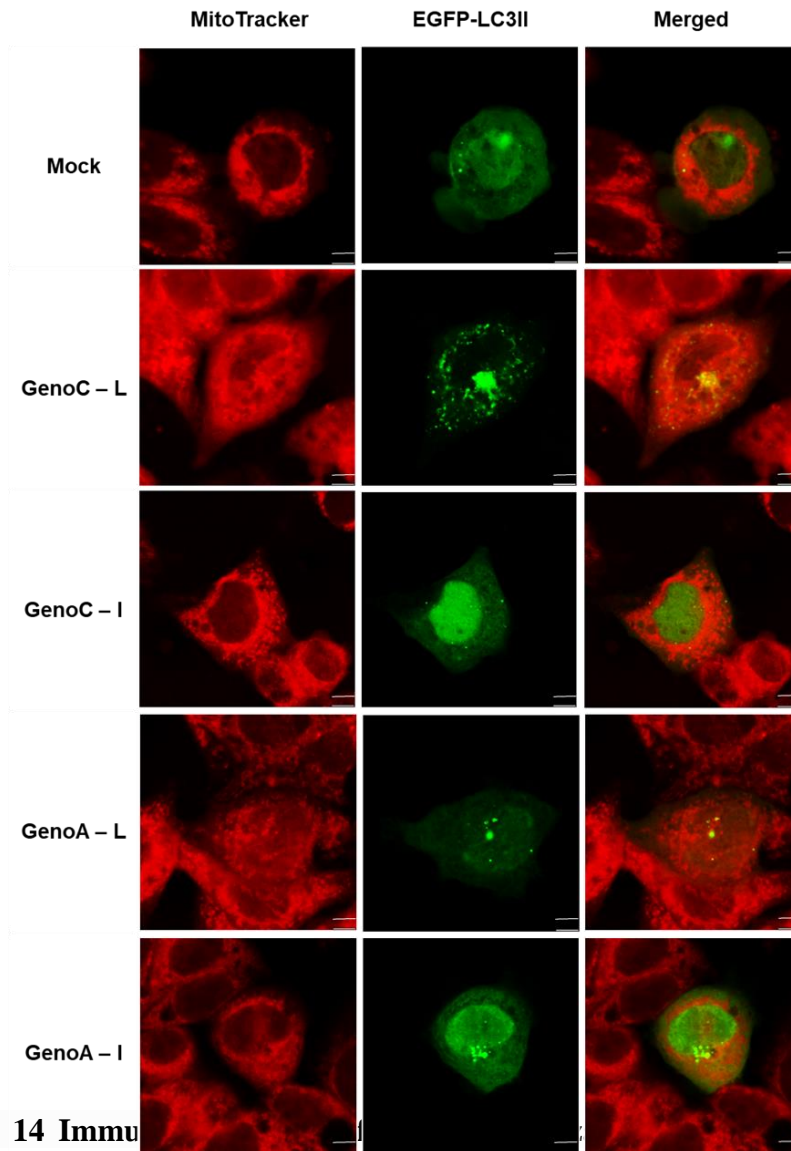


Fig. 14 Immunoautophagosomes with mitochondria EGFP-LC3-expressing vector was cotransfected with HBV genome plasmids. Mitochondria were stained with MitoTracker deep red and yellow dots represent colocalized EGFP-LC3-positive autophagosomes with red labeled mitochondria.

rt269L infection induced mitophagy

For mitochondrial quality control, elimination of damaged organelles, such as mitochondria (mitophagy), is important to maintain normal cellular physiology [27]. To determine whether rt269L is involved in mitophagy, HepG2 cells were cotransfected with EGFP-LC3 and HBV plasmids and stained with MitoTracker red to analyze their colocalization. As shown in Fig. 12C and Fig. 14, I observed that mitochondria in rt269L-infected cells were associated with EGFP LC3 puncta, and their colocalization rates were higher than those of the rt269I type. In addition, the mitophagy-associated protein markers PINK1 and Parkin were significantly increased in rt269L-infected cells (Fig. 12D), suggesting that rt269L-type HBV infection leads to mitophagy induction.

Impaired autophagy in rt269I HBV infection induces caspase activation and cell death by triggering cytochrome c release.

Recent evidence further indicates that impaired autophagy results in increased apoptosis signals, rapid activation of caspase-3, and ultimately cell death [28, 29]. As rt269I-infected cells showed impaired autophagy induction, I hypothesized that rt269I disrupts cellular homeostasis and leads to cell death via caspase activation. To test this hypothesis, I measured active caspase-3 expression through *in vitro* and *in vivo* assays. First, the immunofluorescence data revealed that rt269I-infected cells exhibited the presence of capsase-3-positive compartments (Fig. 15A). In addition, the expression of cleaved caspase-3 protein was markedly increased in rt269I-infected cells (Fig. 15B). Then, I examined liver tissue samples from C57BL/6 mice hydrodynamically injected with rt269L or rt269I HBV to investigate cleaved caspase-3 expression via IHC. Consistently, rt269I-infected mice demonstrated a significant increase in active caspase-3-positive liver cells (Fig. 15C, Fig. 16). Increased cytochrome c release was also detected in mouse liver tissue in the rt269I-infected group, and elevated cytotoxicity as well as ROS were shown in rt269I-infected HepaRG cells and HepG2 cells, respectively (Fig. 15D, Fig. 17).

Furthermore, a TUNEL assay exhibited clear apoptotic features in the liver tissue of rt269I-infected mice (Figs. 18A, Fig. 19), and flow cytometry

analyses showed increased apoptosis of hepatocytes transfected with rt269I HBV (Fig. 18B). Moreover, hematoxylin and eosin (H&E) staining found that rt269I-infected mouse liver tissues exhibited many necrotic hepatocytes and denucleated cells (Fig. 18C). Altogether, impaired autophagy in rt269I infection made cells vulnerable to further elevation of ROS and induced cell death through caspase-3 activation.

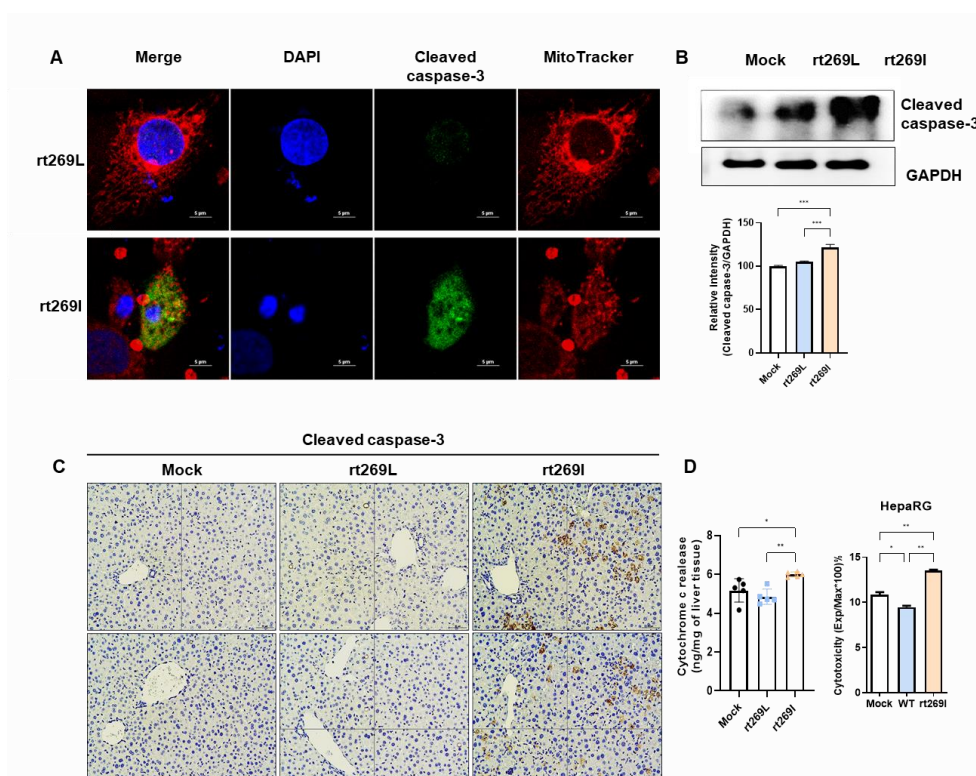


Fig. 15 **rt269I** induces caspase activation and cell death by releasing cytochrome c **A** Confocal images of HepG2 cells transfected with the rt269L or rt269I vector. Green fluorescence represents active (cleaved) caspase-3. Mitochondrial features were stained with MitoTracker, and nuclei were labeled with DAPI. Scale bar: 5 μ m. **B** Western blot analysis of cleaved caspase-3 in HepG2 cells transfected with the rt269L or rt269I vector. The relative intensity of cleaved caspase-3 compared with GAPDH. ***p < 0.001. **C** Immunohistochemistry analysis of cleaved caspase-3 expression in paraffin-embedded liver tissues (magnification 100x, Scale bar = 50 μ m, n=5 per group). **D-left panel** Detection of cytochrome c in liver tissues of mice hydrodynamically injected with mock, rt269L, or rt269I vector and determined by ELISA. **D-right panel** Cytotoxicity levels measured in mock-, rt269L-, or rt269I-type HBV-infected HepaRG cells.

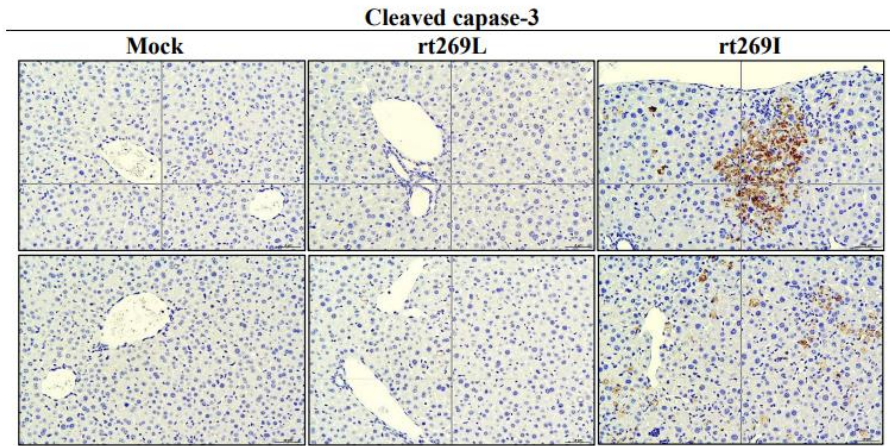


Fig. 16 rt269I HBV induces caspase activation and cell death
Immunohistochemistry analysis of cleaved caspase-3 expression in paraffin-embedded liver tissues (magnification 100x, Scale bar = 50 μ m, n=5 per group).

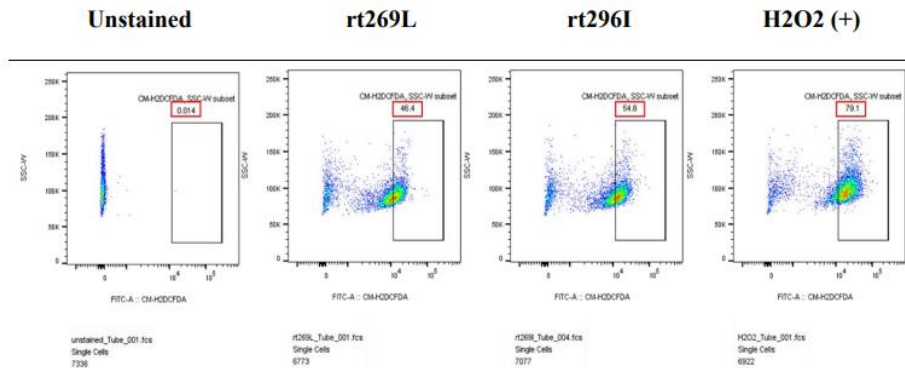


Fig. 17 Detection of intracellular reactive oxygen species in hepatocytes transfected with rt269L or rt269I HBV Reactive oxygen species (ROS) were detected with a CM-H2DCFDA fluorescence probe in hepatocytes transfected with the rt269L or rt269I HBV vector. H2O2 was used as the positive control for ROS induction.

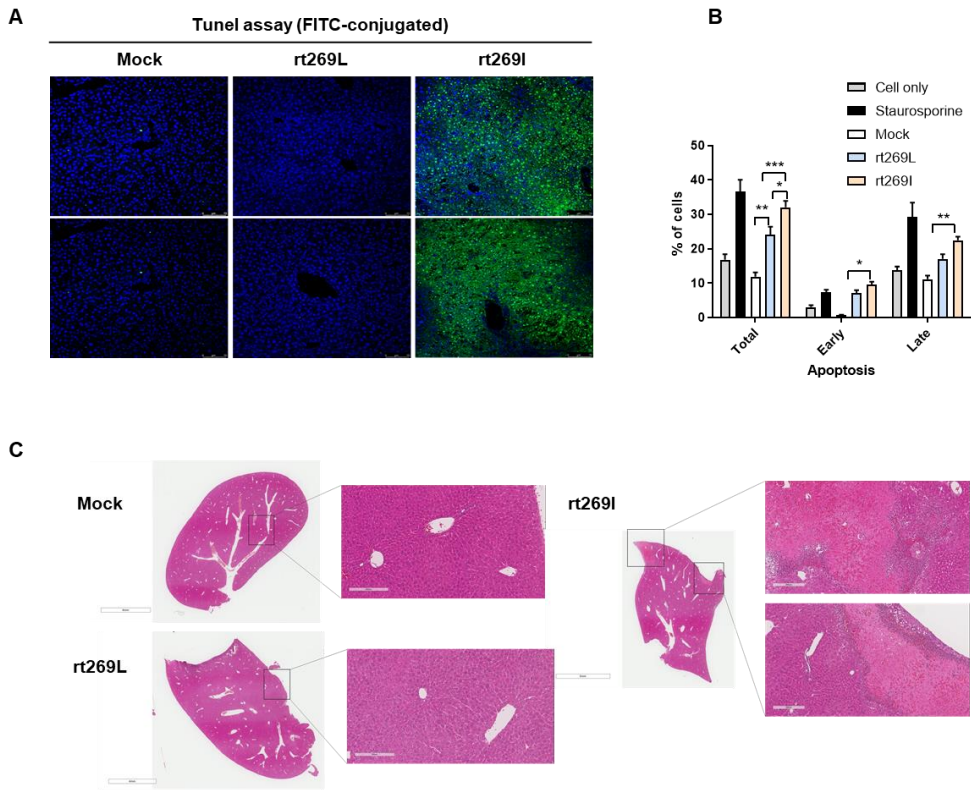


Fig. 18 rt269I induces caspase activation and cell death **A** Cell death in liver tissues of mice hydrodynamically injected with mock, rt269L, or rt269I vector was detected by TUNEL assay (FITC-conjugated). Scale bar = 75 μ m **B** Detection of apoptotic HepG2 cells using Annexin V-FITC and 7-aminoactinomycin D (7-AAD) double-positive assays. Staurosporine (1 μ M) was used to detect the positive control (Con), and the percentage of early or late apoptotic cells is indicated. **C** Mouse liver sections stained with H&E to analyze the liver injury and necrosis area among mouse groups hydrodynamically injected with mock, rt269L, or rt269I HBV. Magnification: 100 \times .

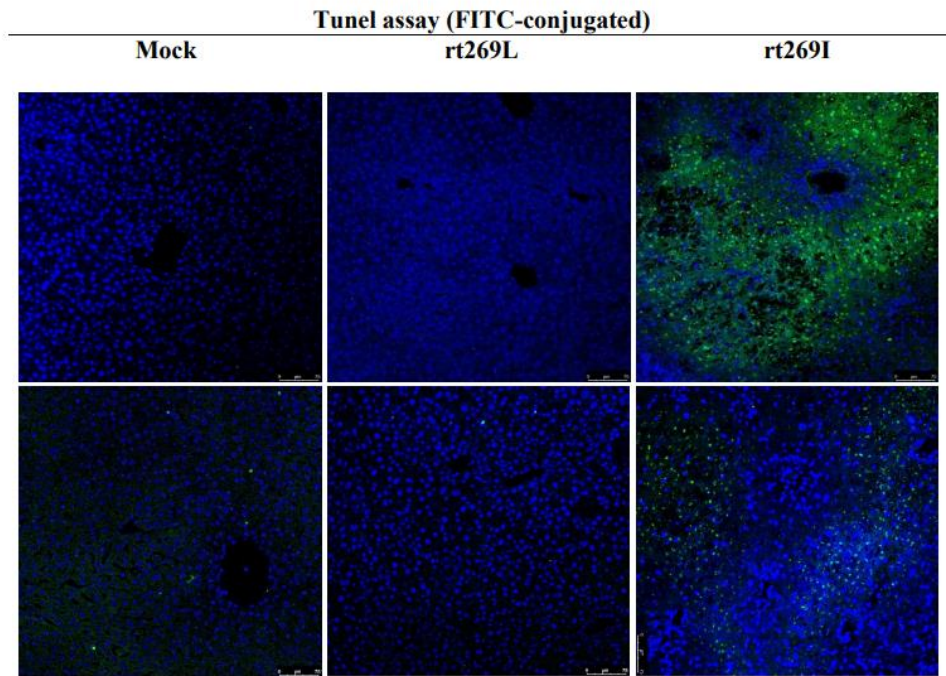


Fig. 19 Cell death in liver tissues of mice hydrodynamically injected with the mock, rt269L, or rt269I vector was detected by TUNEL assay (FITC-conjugated). Nuclei were stained with DAPI (blue). Scale bar = 75 μm .

rt269L infection affects HBx protein levels

I sought to further investigate the underlying mechanisms of the improved mitochondrial functionality and high autophagy induction in rt269L HBV infection. As HBV X protein (HBx) is known to play a central role in resisting cell death via autophagy induction [30-32], I hypothesized that the high capacity to maintain HBx protein in rt269L would be an upstream signaling pathway explaining several characteristics found in HBV genotype C2 infection. First, I tested whether rt269L could affect the HBx protein level. HepG2 cells were cotransfected with HBx-GFP and rt269L or rt269I whole genome plasmids. As shown in Fig. 20A, rt269L significantly increased HBx-GFP expression levels at 48 h post infection. A similar result was obtained in the liver tissue of mice hydrodynamically infected with rt269L HBV (Fig. 20B). In addition, rt269L significantly increased HBx protein levels at 48 h posttransfection in HepG2 cells (Fig. 20C). Interestingly, a similar result was observed in genotype A rt269L, generated by site-directed mutagenesis (Fig. 21A-B). Moreover, HBx protein is known to exert an anti-apoptotic effect via activation of Akt signaling [33, 34], and the data also showed that rt269L infection activated phospho-Akt and phospho-PI3K (Fig.22 and Fig.23).

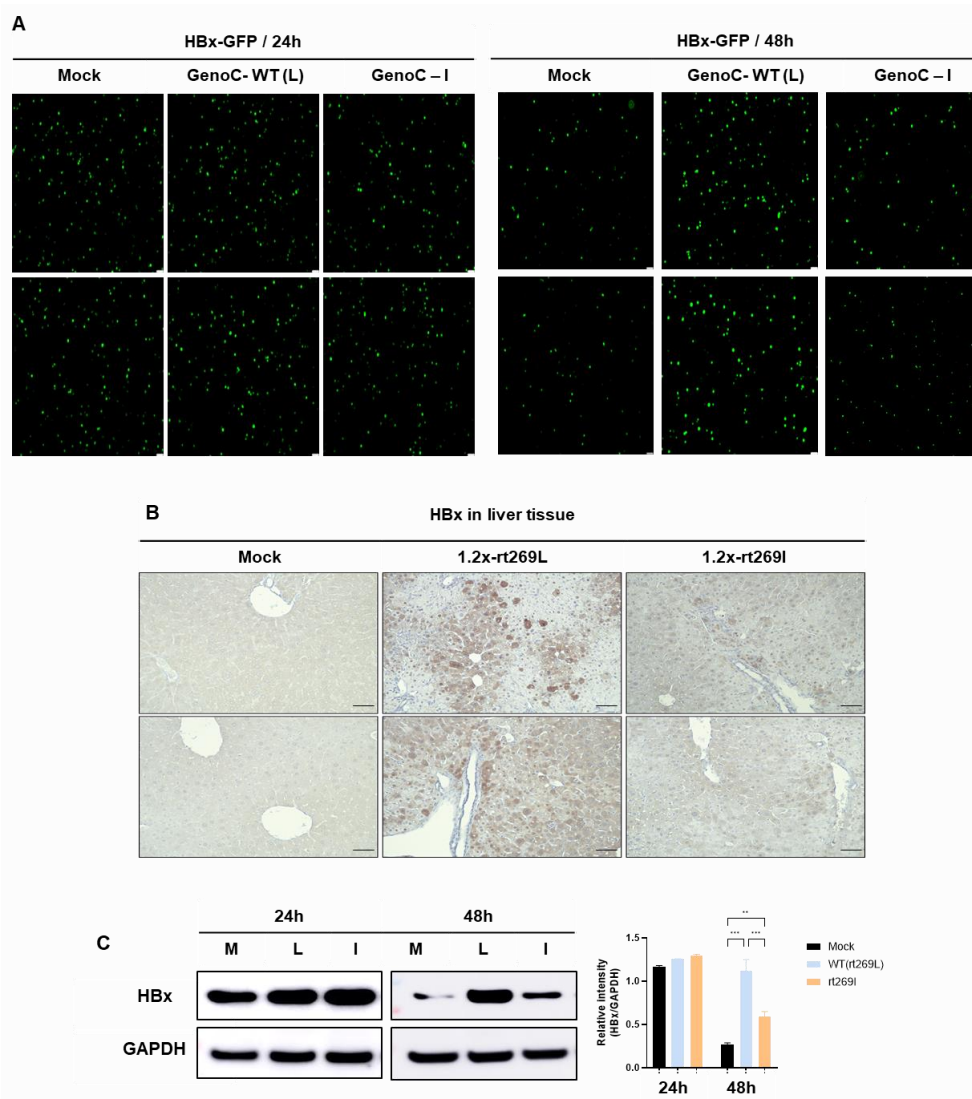


Fig. 20 **rt269L** leads to increased **HBx** protein stability **A** Immunofluorescence images of HBx-GFP expression in HepG2 cells cotransfected with mock, rt269L, and rt269I whole genome plasmids. Scale bar = 100 μ m **B** Immunohistochemical (IHC) analysis of HBx expression in paraffin-embedded liver tissues (magnification 100x, scale bar = 50 μ m, n=5 per group). **C** Western blot analysis of HBx-GFP in HepG2 cells cotransfected with mock, rt269L, or rt269I vector.

promoter region and enhancer I at 48 h. The relative intensity of HBx/GAPDH staining was analyzed. ** $p < 0.01$, *** $p < 0.001$.

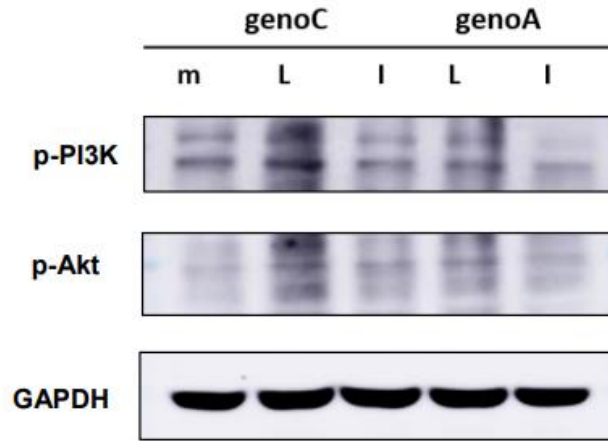


Fig. 22 rt269L type HBV infection in both genotype C and A activated phospho-Akt and phospho-PI3K signals Western blot analysis of the phospho-PI3K and phosphor-Akt, and GAPDH. The relative intensity was analyzed. $**p < 0.01$, $***p < 0.001$.

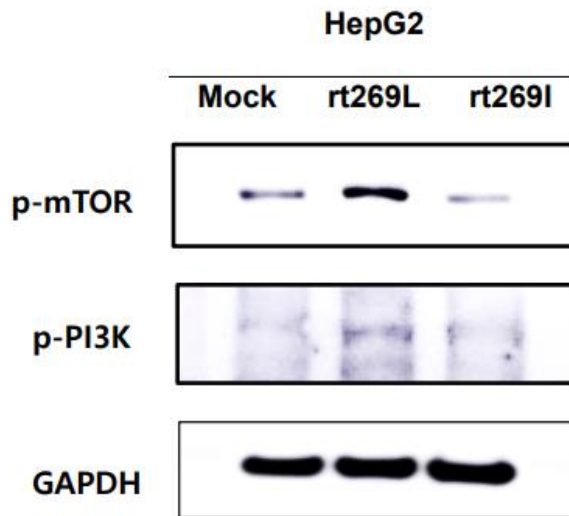


Fig. 23 rt269L type HBV infection activated phospho-mTOR and phospho-PI3K signals in HBx protein dependent manner Western blot analysis of the phospho-PI3K and phosphomTOR, and GAPDH. The relative intensity was analyzed. ** $p < 0.01$, *** $p < 0.001$

Enhanced HBx expression in rt269L activates Enhancer I promoter

Enhancer I (EnhI) is located upstream of and overlaps the X promoter, and it influences the transcription of the HBx gene [35]. To investigate the change in EnhI promoter expression in rt269L, I performed a luciferase reporter assay that measured HBx/EnhI promoter activity [36]. As shown in Fig. 21C, rt269L-cotransfected cells revealed enhanced activation of the HBx/EnhI promoter. Similarly, increased transcription levels of the HBx/EnhI promoter were also shown in rt269L-transfected cells in the genotype A group (Fig. 21C, right panel).

rt269L leads to increased HBx protein stability

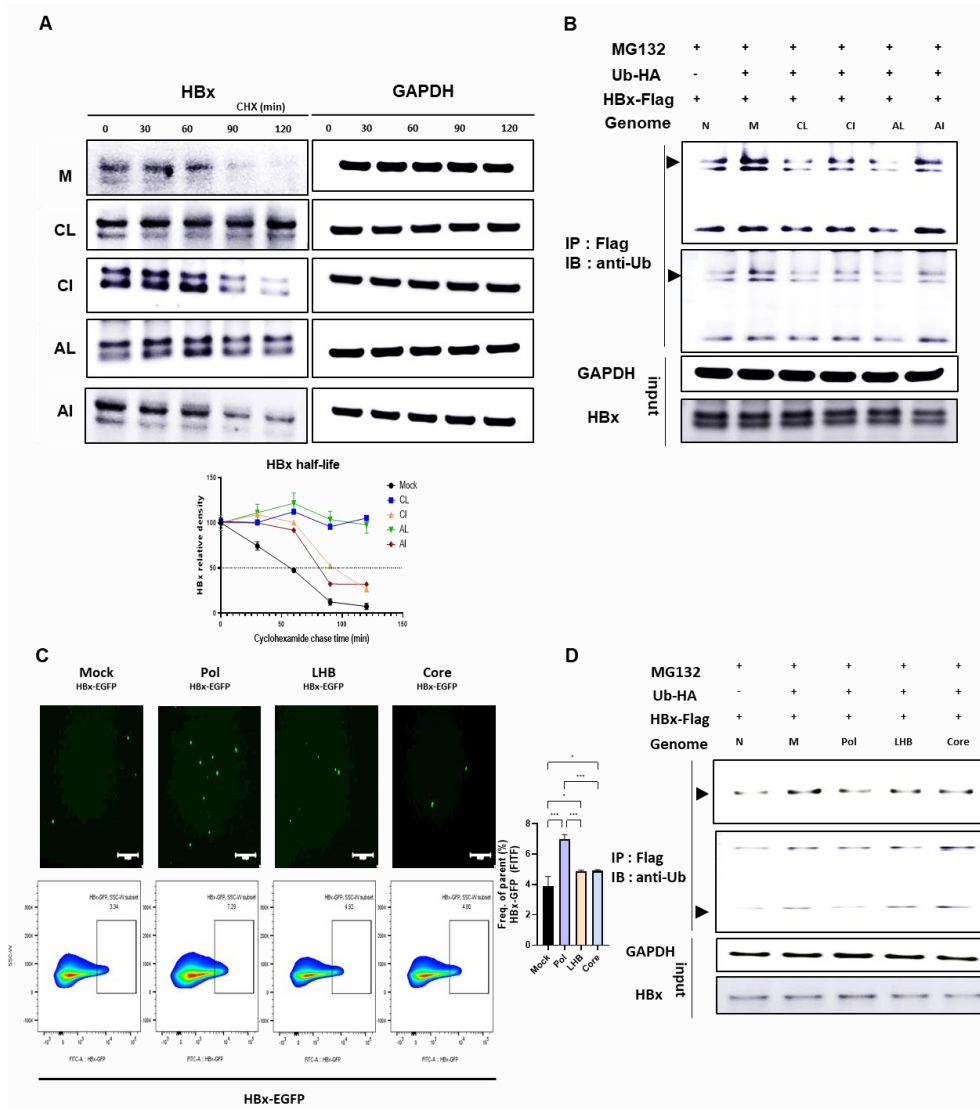
To verify the increase in HBx protein levels in rt269L infection, I performed a cycloheximide chase experiment to determine whether rt269L altered HBx stability. As shown in Fig. 24A, rt269L transfection significantly extended the half-life of HBx protein from approximately 60 min to 120 min in both the genotype A and C groups. These results suggest that rt269L HBV infection leads to enhanced HBx protein stability.

rt269L attenuates HBx degradation through ubiquitination of HBx

HBx turnover can be processed by both ubiquitin-dependent and ubiquitin-independent proteasomal steps [37]. To verify the underlying mechanism of

the enhanced HBx stability in rt269L- infection, I performed a ubiquitination assay by detecting the ubiquitination of HBx proteins with immunoprecipitation. As shown in Fig. 24B, rt269L infection, in both genotypes A and C, revealed diminished ubiquitination of HBx compared with rt269I infection. Then, to clarify the components in the HBV protein that are critical to the stability of the HBx protein, I cloned the Pol (a polymerase), LHB (a large surface protein containing preS1, preS2, and small S), and core ORFs into expression plasmids, and co-expressed each subgenome-containing vector with pGFP-HBx. As shown in Figure 24C, the Pol subgenome group showed significantly increased GFP-HBx expression levels both in fluorescence microscopy images and flow cytometry assays compared with those in the other subgenome groups. In addition, the Pol subgenome-containing vector altered the ubiquitination rate of HBx, in contrast to the other subgenome-containing vectors (Fig. 24D), indicating that the HBV Pol genome and the proteins it encodes are critical for HBx production and ubiquitination. Then, I confirmed that HBx induction is stimulated in a Pol-dependent manner. I generated an rt269L/Pol Δ plasmid (Fig. 26), which does not express Pol, via site-directed mutagenesis and observed HBx expression when the plasmid was co-expressed with pGFP-HBx. As shown in Figure 26A, the rt269L/Pol Δ group showed a reduced GFP-HBx expression level, which was increased in the rt269L group, as

indicated in both the fluorescence microscopy and western blot images. Furthermore, decreased ubiquitination of the HBx protein in the rt269L group was also found (Fig. 26B) when the Pol-rt269 region was deleted by mutagenesis (Fig. 27), and HBx protein stability was measured in a cycloheximide chase experiment after a rt269L-containing Pol subgenome-carrying vector was transfected into HepG2 cells (Fig. 26C). Together, these data indicated a significant role for HBV Pol with rt269L in maintaining HBx protein stability via deubiquitination.



FLAG in combination with mock, rt269L (genotypes A and C), rt269I (genotypes A and C) containing plasmids. Cells were treated with 20 μ M MG132 at 42 h posttransfection for 6 h. Total cell lysates were immunoprecipitated using an anti-FLAG antibody and analyzed by western blotting using an anti-Ubiquitin antibody. **C** Level of HBx-GFP expression of a HBV subgenome-containing plasmid cotransfected into HepG2 cells, as indicated by fluorescence and flow cytometry assays. Scale bar = 200 μ m **D** HepG2 cells were cotransfected with pHBx-FLAG in combination with mock, Pol-, LHB-, and core ORF-containing plasmids. Total cell lysates were immunoprecipitated using an anti-FLAG antibody and analyzed by western blotting using an anti-Ubiquitin antibody.

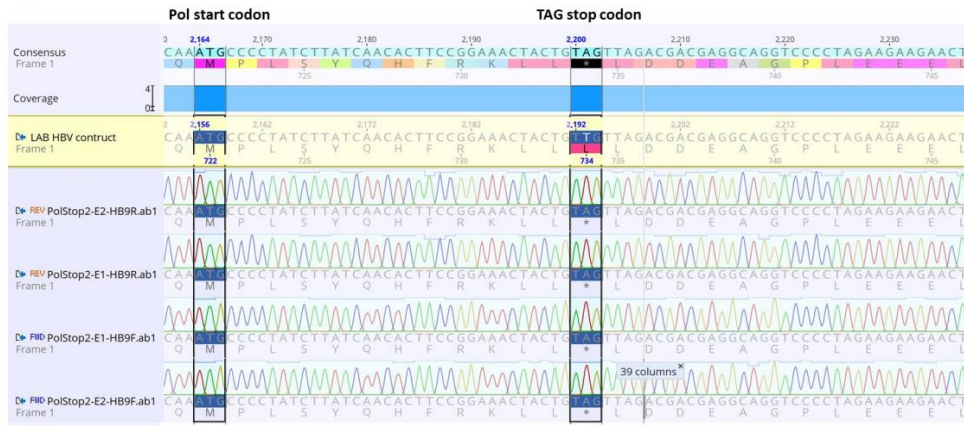


Fig. 25 Site-directed mutagenesis to introduce a stop codon downstream of the Polymerase start region A stop codon was inserted at 36 bp downstream of Polymerase start region (Met) by site-directed point mutation. Converted from TTG to TAG (stop), prevented the translation of full-length Pol region.

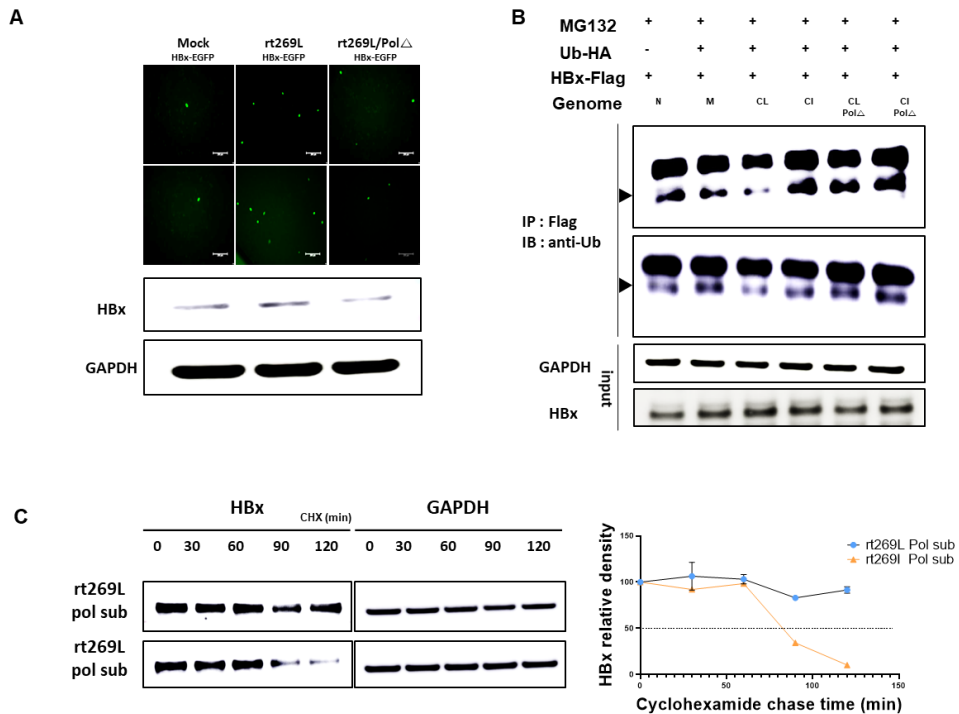


Fig. 26 HBV Pol genome and the proteins it encodes are critical for HBx production and ubiquitination **A** Detection of HBx-GFP protein expression in mock, rt269L, or rt269L/Pol Δ cotransfected HepG2 cells, as shown in fluorescence and western blot assays. Scale bar = 200 μ m **B** HepG2 cells were cotransfected with pHBx-FLAG in combination with mock and Pol-deleted rt269L/I plasmids. Total cell lysates were immunoprecipitated using an anti-FLAG antibody and analyzed by western blotting using an anti-Ubiquitin antibody. **C** A cycloheximide chase experiment with rt269L- or rt269I-containing Pol subgenome-carrying plasmid-transfected cells.



Fig. 27 Site-directed mutagenesis to introduce a stop codon upstream of the rt269 region A stop codon was inserted at 49 bp (887 bp) upstream of rt269 region (936 bp) by site-directed point mutation. Converted from TAT to TAA (stop), prevented the translation of full-length Pol-RT269 region.

Autophagy induction and UPR responses were activated in an HBx-dependent manner

As I verified increased HBx stability in rt269L HBV infection, I examined whether autophagy induction and PERK-eIF2 α -ATF4 signaling were stimulated in an HBx-dependent manner. I generated the rt269L/HBx Δ plasmid by mutagenesis, which does not express HBx protein, and compared the protein expression levels of p-eIF2 α , ATF4 and LC3B in rt269L- and rt269L/HBx Δ transfected HepG2 cells. As shown in Fig. 28A, the increased protein expression levels of p-eIF2 α , ATF4, and LC3B in rt269L cells were diminished in rt269L/HBx Δ transfected cells. A similar result was shown in immunofluorescence images, in which ATF4 expression in rt269L-transfected hepG2 cells was increased, whereas that in rt269L/HBx Δ -transfected cells was reduced (Fig. 28B). In addition, rt269L/HBx Δ dramatically reduced the number of EGFP-LC3B-positive cells as well as the punctuation, indicating that enhanced HBx protein stability in rt269L is an upstream mediator of autophagy induction and UPR responses (Fig. 28C-D).

Elevated hepatic oxidative damage in rt269I HBV infection and its clinical implications

In contrast to rt269L, rt269I infection failed to control mitochondrial quality and showed impaired autophagy induction, which could lead to hepatic

oxidative damage. 8-OHdG is a critical biomarker of oxidative stress and chronic liver disease progression [38]. I observed elevated 8-OHdG levels in the immunofluorescence assay in HepG2 cells transiently transfected with the rt269I vector (Fig. 28E). Similarly, rt269I-infected mouse secreted approximately 1.5-fold higher levels of 8-OHdG compared with the rt269L-injected group (Fig. 28F). I then examined 8-OHdG levels in patients' sera from two different Korean cohorts (Table 3-4), and rt269I-infected patients showed higher 8-OHdG release in their serum than rt269L-infected patients (Fig. 28G). Then, I also tested mitochondrial biomarkers in patient sera from the cohorts. The detection of nDNA fragmentation, mitochondrial DNA and proteins in serum clinically represents mitochondrial damage, liver inflammation, and liver injury [39]. As shown in Fig. 28H, patients infected with rt269I HBV showed more nDNA fragments released in their serum than patients with rt269L HBV infection. Additionally, serum mtDNA release (indicating NADH dehydrogenase activity and cytochrome c oxidation) was 1.5- to 2-fold higher in rt269I-infected patients than in rt269L-infected patients (Fig. 28H). These data suggest that the mitochondrial damage in rt269I-infected patients may be more severe than that in rt269L-infected patients.

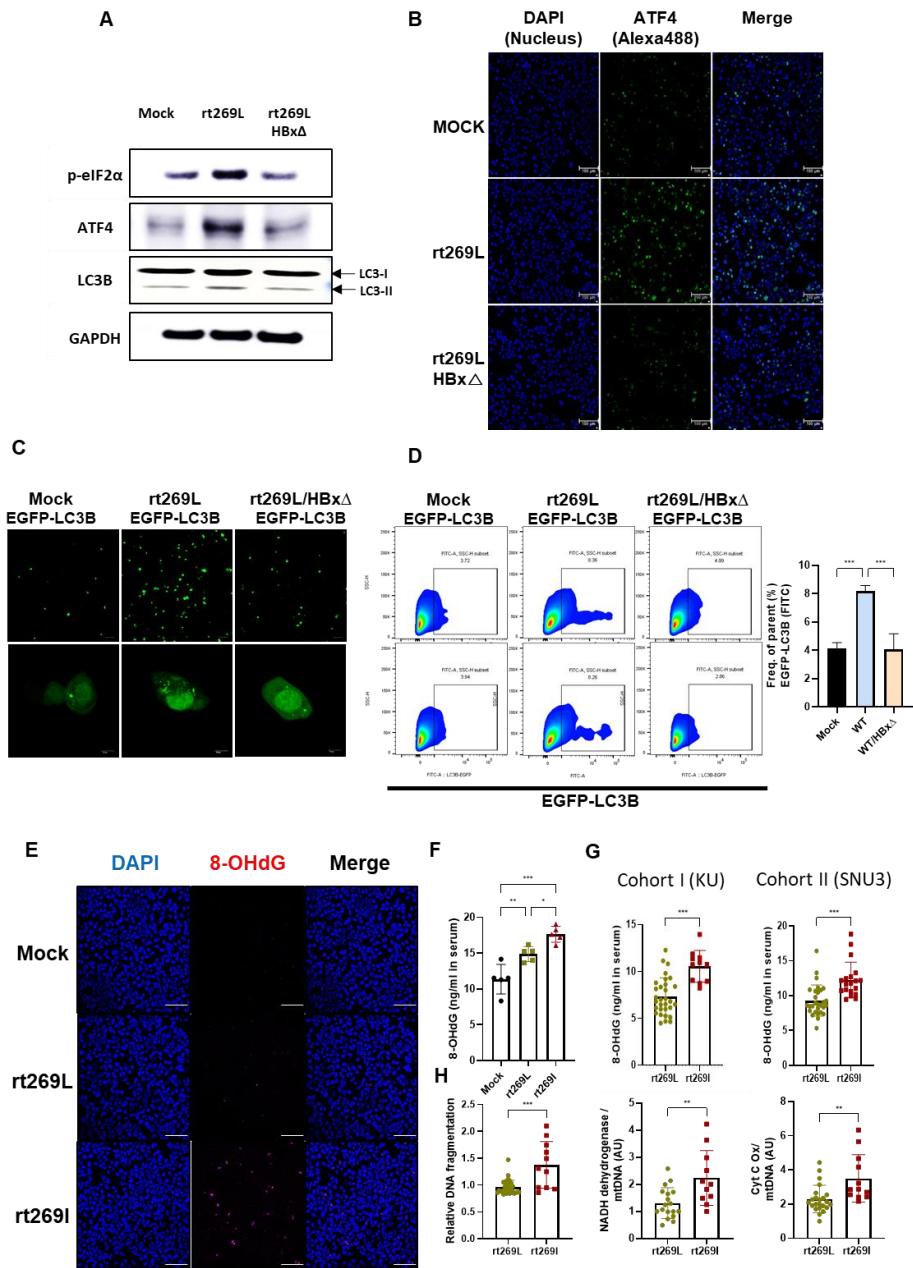


Fig. 28 Elevated hepatic oxidative damage in rt269I HBV infection and its clinical implications

A Western blot analysis of p-eIF2 α , ATF4, LC3B, and GAPDH in HepG2 cells transfected with mock, rt269L, or rt269L/HBx Δ vector. **B** ATF4 expression determined by immunofluorescence assay. Scale bar = 100 μ m. **C-D** Measurement of LC3 puncta after cotransfection of the EGFP-LC3 vector with mock, rt269L-, or rt269L/HBx Δ -containing plasmids, as determined by immunofluorescence and flow cytometry assays. Scale bar = 10 μ m. LC3 is recruited to autophagosomes, forming a punctate structure, as shown by green dots. **E** Formation of 8-OHdG in hepatocytes transfected with rt269I HBV. Representative immunofluorescence images showing 8-OHdG in HepG2 cells transiently transfected with the mock, rt269L, or rt269I vector. Nuclei were stained with DAPI (blue). 8-OHdG, 8-hydroxy-2'-deoxyguanosine. **F** Detection of 8-OHdG release in serum in mice hydrodynamically infected with mock, rt269L, or rt269I vectors. Scale bar = 100 μ m. **G** Measurement of the 8-OHdG release level in patient serum collected from two independent cohorts (KU and SNU3). **H** Mitochondrial damage biomarkers in patient serum. Detection of nuclear DNA (nDNA) fragmentation release in serum detected by ELISA and mitochondrial DNA release in serum detected by RT-qPCR. Scatter dot plots were generated using GraphPad Prism 9.0 software (GraphPad, La Jolla, CA, USA). * p < 0.05, ** p < 0.01, *** p < 0.001.

Table 3. Comparison of clinical factors between two variants in the rt269 codon (KU cohort)

KU (n = 90)	KU (n = 90)		p-value
	rt269L (n=59)	rt269I (n=31)	
Sex (M/F), n (%)	34/25 (57.6/42.4)	19/12 (61.3/38.7)	0.7678
Age (years)	43 [18,73]	44.5 [22,73]	0.3638
HBeAg status (positive, %)	40 (67.8)	17 (54.8)	0.0393*
HBV DNA (log ₁₀ IU/mL)	6.73 [2.78,9.58]	5.99 [3.23,9.43]	0.0147*
qHBsAg (log ₁₀ IU/mL)	3.7 [1.5,5.1]	3.59 [1.4,4.98]	0.1298
AST (IU/L)	59 [16,686]	60 [19,850]	0.8185
ALT (IU/L)	62 [12,659]	63 [10,425]	0.5141
AST/ALT	0.88 [0.34,5.69]	1 [0.35,8.95]	0.1374
Total bilirubin (mg/dL)	0.8 [0.2,6]	1 [0.3,7]	0.0037**
Platelet count (x10 ³ /mm ³)	171 [23,328]	143 [36,350]	0.1839
Albumin (g/dL)	4.1 [2.3,5]	4.3 [2.3,4.8]	0.3845
Prothrombin time (INR)	1.08 [0.87,1.72]	1.11 [0.88,1.79]	0.5236
Presence of LC (no/yes)	39/20 (66.1/33.9)	18/13 (58.1/41.9)	0.2340
Presence of HCC (no/yes)	50/9 (84.7/15.3)	23/8 (74.2/25.8)	0.0734
FIB-4 score	1.54 [0.36,68.71]	2.36 [0.31,26.03]	0.1456

ALT, alanine aminotransferase; AST, aspartate aminotransferase; HBeAg, hepatitis B e antigen; HBsAg, hepatitis B s antigen; HBV DNA, hepatitis B virus DNA; INR, international normalized ratio; qHBsAg, quantitative HBsAg levels; LC, liver cirrhosis; HCC, hepatocellular carcinoma; FIB-4, fibrosis-4. Data represent the frequency and percentage or Med [Min, Max], * $p < 0.05$, ** $p < 0.01$.

Table 4. Comparison of clinical factors between two variants in the rt269 codon (SNU cohort)

SNU3 (n = 97)			
	rt269L (n=68)	rt269I (n=24)	p-value
Sex (M/F), n (%)	54/14 (79.4/20.1)	22/2 (91.7/8.3)	0.17
Age (years)	50.1 [22,72]	53.3 [22,95]	0.25
AST (IU/L)	71.2	64.9	0.83
ALT (IU/L)	65.7 [10,652]	59.4 [10,425]	0.80
AST/ALT	1.10 [0.5,2.41]	1.15 [0.35,8.95]	0.68
Total bilirubin (mg/dL)	1.68	2.67	0.27
Albumin (g/dL)	3.82	3.74	0.64
Globulin (g/dL)	3.36	3.38	0.91
Albumin/Globulin	1.14	1.13	0.90
γ -GTP	44.7	47.3	0.76
Presence of LC (no/yes)	47/21 (69.1/30.9)	14/10 (58.3/41.7)	0.34
Presence of HCC (no/yes)	53/15 (77.9/22.1)	18/6 (75.0/25.0)	0.76

ALT, alanine aminotransferase; AST, aspartate aminotransferase; γ -GTP, gamma-glutamyl transpeptidase; LC, liver cirrhosis; HCC, hepatocellular carcinoma;. Data represent the frequency and percentage or Med [Min, Max].

Discussion

Genotype C, particularly subgenotype C2, is responsible for most chronic infections in HBV-endemic East Asian countries, including China, Japan and Republic of Korea. This genotype is most closely associated with an increased risk of LC and HCC with characteristics including high HBV DNA levels in serum and an elevated tendency for chronicity and mutation [40]. However, the mechanisms underlying these characteristic traits of genotype C infection remain largely unknown. Of note, there are two distinct polymorphisms based on the HBV Pol-269 site, rt269L and rt269I types, in chronic patients with HBV genotype C infection [17]. Recently, I reported that the rt269I HBV genotype C type versus rt269L was more significantly associated with HBeAg-negative seroconversion, liver disease progression, and high mutation rates [17, 18]. In this study, I hypothesized that rt269L infection in the HBV RT region, evident only in genotype C, may play prominent roles in some distinct traits in patients infected with genotype C, including higher infectivity or longer duration of HBeAg positive stage. I sought to explore this issue, focusing on differences in mitochondrial functionality and associated upstream signaling, including ER stress and autophagy induction, between rt269L and rt269I types.

First, I demonstrated that the rt269L mutation leads to increased HBx

protein stability via deubiquitination compared to the rt269I mutation (Fig. 24). Furthermore, this trend is also true in genotype A infection: the genotype A variant with the rt269L mutation in polymerase via mutagenesis also led to enhanced HBx protein stability compared to the wild type (Fig. 24). This finding suggests a significant role of HBV Pol with rt269L in HBx protein stability irrespective of genotype. The HBx protein has multifaceted roles in HBV-related pathogenesis, including HCC or LC progression, as well as viral replication [33, 41, 42]. Of note, it has also been reported to play a very pivotal role in mitochondrial quality control via induction of autophagy/mitophagy [31, 43]. Therefore, the enhanced autophagy/mitophagy induction-mediated improved mitochondrial dynamics and bioenergetics [44] found in rt269L infections in this study (Fig. 1-3 and Fig. 8-9) may be due to enhanced stability of HBx protein, resulting in increased survival of infected hepatocytes, which could contribute to increased HBV replication, persistent infection or longer duration of HBeAg positive phase, distinct traits of genotype C infections. Moreover, HBx protein has been reported to exert an anti-apoptotic effect in infected hepatocytes via activation of Akt signaling [30, 34]. Data also showed that rt269L infection leads to increased Akt-PI3K activation and exerts an anti-apoptotic effect (Fig. 18 and Fig. 22), suggesting a possible contribution of rt269L infection to the increased HCC risk of genotype C

infections.

PERK signaling plays a significant role in the maintenance of mitochondrial homeostasis mainly via the PERK-eIF2 α -ATF4 axis at the interface of the ER and mitochondria during ER stress, alleviating the stress responses of both organelles [13]. Of these, ATF4, a key player in the integrating stress response (ISR), can transcriptionally regulate more than a dozen ATG genes via activation of C/EBP homologous protein (CHOP), a transcription factor, providing a substantial link between autophagy and the UPR [45]. Indeed, the data indicated that rt269L infection can trigger the PERK-eIF2 α -ATF4 axis (Figs. 5-7), in turn contributing to improved mitochondrial dynamics and energetics in infected hepatocytes via autophagy/mitophagy induction (Figs. 1, 3, 8, 9, and 12). In contrast, the rt269I variant failed to trigger PERK signaling during infection, resulting in severe mitochondrial dysfunction via failure of autophagy induction (Fig. 1, 8, and 9).

Notably, dual outcomes of PERK signaling have been described, with PERK playing roles in both cell survival and apoptosis [46, 47]. Genotype C rt269L infection seemed to leverage PERK signaling to promote viral survival and proliferation. I believe that rt269L infection leads to cellular survival and stable replication by increasing mitochondrial functionality via induction of PERK signaling-mediated autophagy, contributing to the high

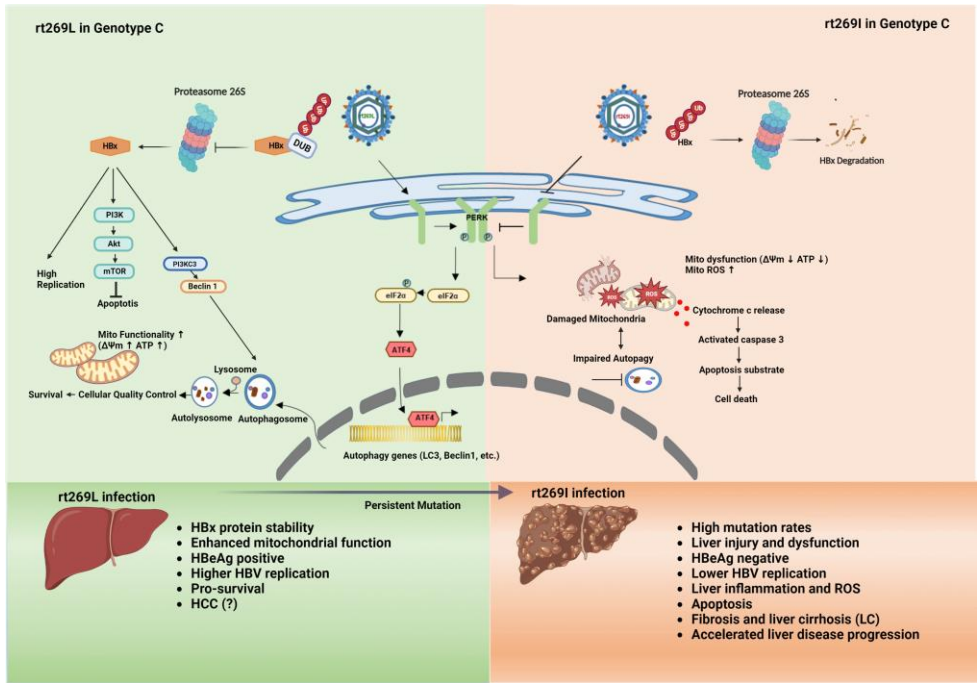
infectivity found in patients with genotype C infections. In contrast, the rt269I HBV variant with impaired PERK signaling leads to altered mitochondrial functionality, contributing to severe hepatic disorders and liver disease progression in patients with genotype C infections. Furthermore, the clinical severity caused by mitochondrial dysfunction and hepatic disorders observed after rt269I infection was also assessed by evaluating the expression of several biomarkers in CHB patient serum (Fig. 28G-H). As mitochondrial contents and DNA fragments detected in plasma are considered clear markers of mitochondrial injury and DNA fragmentation, respectively, particularly in necrotic cells [48], higher levels of 8-OHdG, DNA fragments, and mtDNA release of rt269I infections (Fig. 28G-H) found in Korean patient sera further support the hypothesis associated with poor clinical outcomes for patients with genotype C2 rt269I infection.

Taking these findings together, I verified that HBx stability and cellular quality control mediated via autophagy in the rt269L (WT) type group may indicate a major reason for the clinical features of genotype C infection, such as high replication and infection rates, sustained cccDNA, and a lower response to IFN therapy. Meanwhile, as the high infectivity of rt269L was retained, leading to chronic infection, the rt269I-type variant developed and showed increasingly higher mutation rates, leading to liver disease

progression. Functional differences at the molecular level between rt269L and rt269I in HBV genotype C infection need to be further characterized in the future, which could provide new insight into developing a novel therapeutic strategy for HBV genotype C infection.

Conclusion

In conclusion, the data showed that the rt269L type presented exclusively in HBV genotype C infection versus rt269I common in other genotypes leads to improved mitochondrial dynamics or bioenergetics, which is mainly due to autophagy induction via activation of the PERK–eIF2 α –ATF4 axis in an HBx protein-dependent manner. This suggests that rt269L type predominating in genotype C endemic areas could at least partly contribute to some distinct traits of genotype C infection, such as higher infectivity or longer duration of HBeAg positive stage. In contrast, the rt269I variant in HBV genotype C infection is significantly associated with mitochondrial dysfunction and impaired autophagy due to impaired PERK signaling, resulting in enhanced ROS production and apoptosis in infected hepatocytes. CHB patients infected with the rt269I variant of genotype C likely have increased risks of LC caused by hepatic disorder, ROS leakage, ATP deficiency, and severe DNA damage compared to those with rt269L HBV (Schematic figure).



Schematic figure

References

- 1 Organization WH Global diffusion of eHealth: making universal health coverage achievable: report of the third global survey on eHealth, World Health Organization, 2017.
- 2 Wang M, Ma X, Wang G, Song Y, Zhang M, Mai Z, et al. Targeting UBR5 in hepatocellular carcinoma cells and precise treatment via echinacoside nanodelivery. *Cellular & Molecular Biology Letters*. 2022;27:92.
- 3 Organization WH. Global Hepatitis Report 2017.[cited 15 April 2021]. World Health Organization [Internet]. Available from: <https://www.who.int/hepatitis/publications/global-hepatitis-report2017/en>.
- 4 KAO JH. Hepatitis B viral genotypes: clinical relevance and molecular characteristics. *Journal of gastroenterology and hepatology*. 2002;17:643-650.
- 5 Lin C-L and Kao J-H. Natural history of acute and chronic hepatitis B: The role of HBV genotypes and mutants. *Best Practice & Research Clinical Gastroenterology*. 2017;31:249-255.
- 6 Chan HLY, Wong GLH, Tse CH, Chim AML, Yiu KKL, Chan HY, et al. Hepatitis B virus genotype C is associated with more severe liver fibrosis than genotype B. *Clinical gastroenterology and hepatology*. 2009;7:1361-1366.
- 7 McMahan BJ, Nolen LD, Snowball M, Homan C, Negus S, Roik E, et al. HBV genotype: a significant risk factor in determining which patients with chronic HBV infection should undergo surveillance for HCC: the hepatitis B Alaska study. *Hepatology*. 2021;74:2965-2973.
- 8 Spinelli JB and Haigis MC. The multifaceted contributions of mitochondria to cellular metabolism. *Nature cell biology*. 2018;20:745-754.
- 9 Palikaras K, Lionaki E and Tavernarakis N. Mechanisms of mitophagy in cellular homeostasis, physiology and pathology. *Nature cell biology*. 2018;20:1013-1022.
- 10 Kim S-J, Ahn D-G, Syed GH and Siddiqui A. The essential role of mitochondrial dynamics in antiviral immunity. *Mitochondrion*. 2018;41:21-27.
- 11 Sedlackova L and Korolchuk VI. Mitochondrial quality control as a key determinant of cell survival. *Biochimica et Biophysica Acta (BBA)-Molecular Cell Research*. 2019;1866:575-587.
- 12 Choi Y-M, Lee S-Y and Kim B-J. Naturally occurring hepatitis B virus mutations leading to endoplasmic reticulum stress and their contribution to the progression of hepatocellular carcinoma. *International journal of molecular sciences*. 2019;20:597.
- 13 Senft D and Ze'ev AR. UPR, autophagy, and mitochondria crosstalk underlies the ER stress response. *Trends in biochemical sciences*. 2015;40:141-148.
- 14 Luhr M, Torgersen ML, Szalai P, Hashim A, Brech A, Staerk J, et al. The kinase PERK and the transcription factor ATF4 play distinct and essential roles in

autophagy resulting from tunicamycin-induced ER stress. *Journal of Biological Chemistry*. 2019;294:8197-8217.

15 Bartoszewska S and Collawn JF. Unfolded protein response (UPR) integrated signaling networks determine cell fate during hypoxia. *Cellular & molecular biology letters*. 2020;25:1-20.

16 Lebeau J, Saunders JM, Moraes VW, Madhavan A, Madrazo N, Anthony MC, et al. The PERK arm of the unfolded protein response regulates mitochondrial morphology during acute endoplasmic reticulum stress. *Cell reports*. 2018;22:2827-2836.

17 Lee S-Y, Choi Y-M, Oh S-J, Yang S-B, Lee J, Choe W-H, et al. rt269I type of hepatitis B virus (HBV) leads to HBV e antigen negative infections and liver disease progression via mitochondrial stress mediated type I interferon production in chronic patients with genotype C infections. *Frontiers in immunology*. 2019;17:35.

18 Jeong H, Kim DH, Choi Y-M, Choi H, Kim D and Kim B-J. Rt269i type of hepatitis b virus (Hbv) polymerase versus rt269I is more prone to mutations within hbv genome in chronic patients infected with genotype c2: Evidence from analysis of full hbv genotype c2 genome. *Microorganisms*. 2021;9:601.

19 Chapman J, Ng YS and Nicholls TJ. The maintenance of mitochondrial DNA integrity and dynamics by mitochondrial membranes. *Life*. 2020;10:164.

20 LeBleu VS, O'Connell JT, Gonzalez Herrera KN, Wikman H, Pantel K, Haigis MC, et al. PGC-1 α mediates mitochondrial biogenesis and oxidative phosphorylation in cancer cells to promote metastasis. *Nature cell biology*. 2014;16:992-1003.

21 Xia M, Zhang Y, Jin K, Lu Z, Zeng Z and Xiong W. Communication between mitochondria and other organelles: a brand-new perspective on mitochondria in cancer. *Cell & Bioscience*. 2019;9:1-19.

22 Wortel IM, van der Meer LT, Kilberg MS and van Leeuwen FN. Surviving stress: modulation of ATF4-mediated stress responses in normal and malignant cells. *Trends in Endocrinology & Metabolism*. 2017;28:794-806.

23 B'chir W, Maurin A-C, Carraro V, Averous J, Jousse C, Muranishi Y, et al. The eIF2 α /ATF4 pathway is essential for stress-induced autophagy gene expression. *Nucleic acids research*. 2013;41:7683-7699.

24 Guo F, Zhang H, Chen C, Hu S, Wang Y, Qiao J, et al. Autophagy favors *Brucella melitensis* survival in infected macrophages. *Cellular and Molecular Biology Letters*. 2012;17:249-257.

25 Sir D, Tian Y, Chen W-l, Ann DK, Yen T-SB and Ou J-hj. The early autophagic pathway is activated by hepatitis B virus and required for viral DNA replication. *Proceedings of the National Academy of Sciences*. 2010;107:4383-4388.

26 Mao J, Lin E, He L, Yu J, Tan P and Zhou Y. Autophagy and viral infection. *Autophagy regulation of innate immunity*. 2019;55-78.

27 Pickles S, Vigié P and Youle RJ. Mitophagy and quality control mechanisms in mitochondrial maintenance. *Current Biology*. 2018;28:R170-R185.

- 28 Ogata M, Hino S-i, Saito A, Morikawa K, Kondo S, Kanemoto S, et al. Autophagy is activated for cell survival after endoplasmic Reticulum Stress. *Molecular and cellular biology*. 2006;26:9220-9231.
- 29 Chung Y, Lee J, Jung S, Lee Y, Cho JW and Oh YJ. Dysregulated autophagy contributes to caspase-dependent neuronal apoptosis. *Cell death & disease*. 2018;9:1-19.
- 30 Wang P, Guo Q-s, Wang Z-w and Qian H-x. HBx induces HepG-2 cells autophagy through PI3K/Akt-mTOR pathway. *Molecular and Cellular Biochemistry*. 2013;372:161-168.
- 31 Son J, Kim M-J, Lee JS, Kim JY, Chun E and Lee K-Y. Hepatitis b virus x protein promotes liver cancer progression through autophagy induction in response to tlr4 stimulation. *Immune Network*. 2021;21.
- 32 Zhang Z, Han Y, Sun G, Liu X, Jia X and Yu X. MicroRNA-325-3p inhibits cell proliferation and induces apoptosis in hepatitis B virus-related hepatocellular carcinoma by down-regulation of aquaporin 5. *Cellular & molecular biology letters*. 2019;24:1-15.
- 33 Rawat S and Bouchard MJ. The hepatitis B virus (HBV) HBx protein activates AKT to simultaneously regulate HBV replication and hepatocyte survival. *Journal of virology*. 2015;89:999-1012.
- 34 Wang X, Huo B, Liu J, Huang X, Zhang S and Feng T. Hepatitis B virus X reduces hepatocyte apoptosis and promotes cell cycle progression through the Akt/mTOR pathway in vivo. *Gene*. 2019;691:87-95.
- 35 Slagle BL and Bouchard MJ. Hepatitis B virus X and regulation of viral gene expression. *Cold Spring Harbor perspectives in medicine*. 2016;6:a021402.
- 36 Kim W, Lee S, Son Y, Ko C and Ryu W-S. DDB1 stimulates viral transcription of hepatitis B virus via HBx-independent mechanisms. *Journal of virology*. 2016;90:9644-9653.
- 37 Wu Q, Zhang L, Xu X, Zhang Y, Shi J, Lin X, et al. Hepatitis B Virus X Protein Is Stabilized by the Deubiquitinating Enzyme VCPIP1 in a Ubiquitin-Independent Manner by Recruiting the 26S Proteasome Subunit PSMC3. *Journal of Virology*. 2022;96:e00611-00622.
- 38 Valavanidis A, Vlachogianni T and Fiotakis C. 8-hydroxy-2' - deoxyguanosine (8-OHdG): a critical biomarker of oxidative stress and carcinogenesis. *Journal of environmental science and health Part C*. 2009;27:120-139.
- 39 McGill MR, Staggs VS, Sharpe MR, Lee WM, Jaeschke H and Group ALFS. Serum mitochondrial biomarkers and damage - associated molecular patterns are higher in acetaminophen overdose patients with poor outcome. *Hepatology*. 2014;60:1336-1345.
- 40 Sunbul M. Hepatitis B virus genotypes: global distribution and clinical importance. *World journal of gastroenterology: WJG*. 2014;20:5427.

- 41 Gao Y, Gu J, Wang Y, Fu D, Zhang W, Zheng G, et al. Hepatitis B virus X protein boosts hepatocellular carcinoma progression by downregulating microRNA-137. *Pathology-Research and Practice*. 2020;216:152981.
- 42 Wang X, Wei Z, Jiang Y, Meng Z and Lu M. mTOR Signaling: The Interface Linking Cellular Metabolism and Hepatitis B Virus Replication. *Virologica Sinica*. 2021;1-12.
- 43 Lei Y, Xu X, Liu H, Chen L, Zhou H, Jiang J, et al. HBx induces hepatocellular carcinogenesis through ARRB1-mediated autophagy to drive the G1/S cycle. *Autophagy*. 2021;17:4423-4441.
- 44 Ma K, Chen G, Li W, Kepp O, Zhu Y and Chen Q. Mitophagy, mitochondrial homeostasis, and cell fate. *Frontiers in cell and developmental biology*. 2020;8:467.
- 45 Pakos - Zebrocka K, Koryga I, Mnich K, Ljujic M, Samali A and Gorman AM. The integrated stress response. *EMBO reports*. 2016;17:1374-1395.
- 46 Siwecka N, Rozpędek W, Pytel D, Wawrzynkiewicz A, Dziki A, Dziki Ł, et al. Dual role of endoplasmic reticulum stress-mediated unfolded protein response signaling pathway in carcinogenesis. *International journal of molecular sciences*. 2019;20:4354.
- 47 Faitova J, Krekac D, Hrstka R and Vojtesek B. Endoplasmic reticulum stress and apoptosis. *Cellular & molecular biology letters*. 2006;11:488-505.
- 48 McGill MR, Sharpe MR, Williams CD, Taha M, Curry SC and Jaeschke H. The mechanism underlying acetaminophen-induced hepatotoxicity in humans and mice involves mitochondrial damage and nuclear DNA fragmentation. *The Journal of clinical investigation*. 2012;122:1574-1583.

국문 초록

배경: 본 연구자는 선행연구를 통해 HBV C2 유전자형 감염에서 rt269I 유형이 rt269L 유형 감염에 비해 간 질환의 발전을 초래하고 감염된 간세포에서 미토콘드리아 스트레스를 증가시키는 것을 확인하였음. 본 연구에서는 HBV genotype C2 감염에서 rt269L 유형과 rt269I 유형 간의 미토콘드리아 기능 차이를 규명하고자 하였음. 본 연구는 주로 ER 스트레스 매개 오토파지 유도를 상위 신호로 하는 미토콘드리아 기능에 초점을 맞추어 진행하였음.

연구방법: rt269L 유형과 rt269I 유형 그룹 간의 미토콘드리아 기능, ER 스트레스 신호, 오토파지 유도 및 세포 자살 등을 vitro 및 in vivo 실험을 통해 규명하였음. 또한 건국대 병원 및 서울대 병원의 187명의 만성 간염 환자에서 혈청 샘플을 수집하여 분석하였음.

연구결과: HBV 유전자형 C rt269L 타입 감염은 PERK-eIF2 α -ATF4 축의 ER stress를 활성화함으로써 개선된 미토콘드리아 기능 및 오토파지를 유도하는 것을 확인하였음. 또한, rt269L 감염에서 관찰된 특성이 HBx 단백질의 유비퀴틴을 저해함으로써 안정성을 증가시켜 증대되는 것임을 입증하였음. 더불어, 두 독립적인 한국 코호트의 환자 혈청을 사용한 임상 데이터에 따르면 rt269I에 비해 rt269L의 감염은

낮은 8-OHdG 발현 수치를 보임으로써 rt269L 타입 감염이 미토콘드리아 질적 기능을 개선하는 것을 확인하였음.

결론: rt269L형 HBV 감염은 주로 HBx 단백질 의존적으로 PERK-eIF2 α -ATF4 축의 활성화를 통한 오토파지 유도로 인해 미토콘드리아 역학 또는 생체 에너지 개선으로 이어짐을 규명하였음. 이것은 유전자형 C 만연 지역에서 우세한 rt269L 유형의 HBx 단백질 안정성 및 세포 기능 및 질적 관리가 부분적으로 높은 감염성 또는 HBeAg 양성 단계의 더 긴 지속 시간과 같은 유전자형 C 감염의 독특한 특성에 기여할 수 있음을 시사함.